(2)

AD

AD-A153 654

B
R
L

CONTRACT REPORT BRL-CR-540

A NEW INTERACTION ALGORITHM WITH EROSION FOR EPIC-3

Ted Belytschko Inc.
18 Longmeadow Road
Winnetka, IL 60093

February 1985

US ARMY BALLISTIC RESEARCH LABORATORY
ABERDEEN PROVING GROUND, MARYLAND

Destroy this report when it is no longer needed.
Do not return it to the originator.

Additional copies of this report may be obtained from the National Technical Information Service, U. S. Department of Commerce, Springfield, Virginia 22161.

The findings in this report are not to be construed as an official Department of the Army position, unless so designated by other authorized documents.

The use of trade names or manufacturers' names in this report does not constitute indorsement of any commercial product.

UNCLASSIFIED

SECURITY CLASSIFICATION OF THIS PAGE (When Data Entered)

REPORT DOCUMENTATION PAGE

READ INSTRUCTIONS BEFORE COMPLETING FORM

1. REPORT NUMBER: CONTRACT REPORT BRL-CR-540	2. GOVT ACCESSION NO.: AD A153654
3. RECIPIENT'S CATALOG NUMBER:	
4. TITLE (and Subtitle): A New Interaction Algorithm with Erosion for EPIC-3	5. TYPE OF REPORT & PERIOD COVERED: Final, March 1983 - March 1984
	6. PERFORMING ORG. REPORT NUMBER:
7. AUTHOR(s): T. Belytschko, J. I. Lin	8. CONTRACT OR GRANT NUMBER(s): DAAK11-83-C-0020
9. PERFORMING ORGANIZATION NAME AND ADDRESS: Ted Belytschko Inc., 18 Longmeadow Rd., Winnetka, IL 60093	10. PROGRAM ELEMENT, PROJECT, TASK AREA & WORK UNIT NUMBERS: 1L162618AH80
11. CONTROLLING OFFICE NAME AND ADDRESS: US Army Ballistic Research Laboratory, ATTN: AMXBR-ST-OD, Aberdeen Proving Ground, MD 21005-5066	12. REPORT DATE: February 1985
	13. NUMBER OF PAGES: 62
14. MONITORING AGENCY NAME & ADDRESS (if different from Controlling Office)	15. SECURITY CLASS. (of this report): UNCLASSIFIED
	15a. DECLASSIFICATION/DOWNGRADING SCHEDULE:

16. DISTRIBUTION STATEMENT (of this Report)

Approved for public release; distribution unlimited.

17. DISTRIBUTION STATEMENT (of the abstract entered in Block 20, if different from Report)

18. SUPPLEMENTARY NOTES

19. KEY WORDS (Continue on reverse side if necessary and identify by block number)

EPIC-3
Impact
Ballistics
Eroding Slidelines
Penetrators
Finite Elements

20. ABSTRACT (Continue on reverse side if necessary and identify by block number)

This report documents modifications which were incorporated in the EPIC-3 [5,6] computer program (Elastic-Plastic Impact Computations in Three Dimensions) in order to treat impact and penetration with erosion. EPIC-3 is a finite element program with explicit time integration which is primarily intended for simulation of solids to short intense loads, such as in impact or explosive detonations. A variety of material laws including elastic-plastic solids, concrete/geological materials and explosives are included.

DD FORM 1 JAN 73 1473 EDITION OF 1 NOV 65 IS OBSOLETE

UNCLASSIFIED

SECURITY CLASSIFICATION OF THIS PAGE (When Data Entered)

As part of this modification, two major features were added:

1. A hexahedral element with one-point quadrature and hourglass control;
2. An algorithm for treating projectile-target interaction in situations where material erosion can occur arbitrarily in the target or projectile.

A key attribute of the interaction algorithm is that it requires no definition or tracking of sliding interfaces. Instead, the interaction is handled by operations on slave nodes and master elements. Because of this feature of the algorithm, the erosion of an element requires no redefinition of the interface and thus avoids the complexity associated with sliding interfaces in these situations. The hexahedral element was incorporated primarily because it simplifies the new interaction algorithm. However, it also increases the speed of the computer program and avoids the excessive stiffness of the tetrahedra.

Solutions are presented for three projectile penetration problems, ranging from a simple problem primarily intended to verify the computer code to a large-scale problem involving erosion of both the projectile and target.

TABLE OF CONTENTS

LIST OF FIGURES

INTRODUCTION

This report documents modifications which were incorporated in the EPIC-3 [5,6] computer program (Elastic-Plastic Impact Computations in Three Dimensions) in order to treat impact and penetration with erosion. EPIC-3 is a finite element program with explicit time integration which is primarily intended for simulation of solids subjected to short intense loads, such as in impact or explosive detonations. A variety of material laws including elastic-plastic solids, concrete/geological materials and explosives are included.

As part of this modification, two major features were added:

1. a hexahedral element with one-point quadrature and hourglass control;
2. an algorithm for treating projectile-target interaction in situations where material erosion can occur arbitrarily in the target or projectile.

The hexahedral finite element is an isoparametric element with 8 nodes and 24 degrees of freedom. The stresses and strains are evaluated only at a single point in the element, which makes certain physically unrealistic modes of deformation, known as hourglass modes, possible. These are avoided here by the use of hourglass control.

A key attribute of the interaction algorithm is that it requires no definition or tracking of sliding interfaces. Instead, the interaction is handled by operations on slave nodes and master elements. Because of this feature of the algorithm, the erosion of an element requires no redefinition of the interface and thus avoids the complexity associated with sliding interfaces in these situations. The hexahedral element was incorporated primarily because it simplifies the new interaction algorithm. However, it also increases the speed of the computer program and avoids the excessive stiffness of the tetrahedra.

The element is described in Section 2, the interaction algorithm in Section 3. Section 3 describes some sample problems which were solved by this algorithm. The modified input manual is given in Section 4. Equations in this report are numbered by section and sub-section, so that each equation number consists of 3 numbers: the section number, the sub-section number, and the number of the equation with the sub-section. However, when referring to an equation, the first number, the section number, is included only when the equation is in a <u>different</u> section.

Section 1

HEXAHEDRAL ELEMENT

1.1 Overview and Notation

The hexahedral element consists of 8 nodes and 6 sides as shown in Fig. 1. The positions of the nodes are completely arbitrary although the local node numbering must be in accord with the following convention:

i) nodes 1 to 4 must be placed sequentially on a single surface so that the thumb of the right hand points to the interior of the element when the fingers follow the nodes in sequence;

ii) nodes 5 to 8 must each be connected by edges to nodes 1 to 4, respectively; i.e., nodes 1 and 5, 2 and 6, 3 and 7 and 4 and 8 must each lie on the same edge.

The element is an isoparametric element with the displacement field defined in terms of the coordinates of reference cube in ξ, η, ζ space, see Fig. 1. In terms of the reference coordinate system, the displacement and velocity field are trilinear, with none of the coordinates appearing in the polynomial in a power higher than linear. The resulting strain fields are then bilinear.

However, only one quadrature point is used in evaluating the strain and stress fields in the element. This implies that for purposes of evaluating the nodal forces, the strain-rates and stresses are considered constant.

The assumption of a constant stress field implies that certain deformation modes of the element will not be resisted by nodal forces; this phenomenon is known as hourglassing; see Ref. [1]. To avoid the severe mesh distortions brought about by hourglassing, an hourglass procedure developed by Flanagan and Belytschko [2] will be used. This hourglassing procedure is advantageous in that it does not compromise the formal consistency of the resulting difference equations, so convergence is not impaired; see Ref. [1].

In the following, we first give the fundamental equations for the hexahedral element. Two types of $\underset{\sim}{B}$ matrices for one-point quadrature have been incorporated; one is based on centroidal evaluations of the $\underset{\sim}{B}$ matrix as in Ref. [3] the second is based on the uniform strain procedure given in Ref. [2]. The centroidal method is cheaper but loses accuracy as the element distorts. In particular, if the element is degenerated to a pentahedron or tetrahedron, it becomes very inaccurate, whereas the Flanagan-Belytschko formulas [2] remain exact.

After the development of the $\underset{\sim}{B}$-matrices, the hourglass control procedure is given. Then the formulas for estimating the stable time steps based on Ref. [4], which are used for the hexahedron, are presented.

Standard indicial notation will be used in this report. Lower case Latin indices pertain to components and have a range of three; when they are repeated a summation over their range is implied. Upper case indices pertain to nodes of an element and have a range of 8. The range of Greek letters is specified whenever they are used. Commas denote derivatives with respect to the spatial variables, i.e. $f_{,i} = \partial f/\partial x_i$.

Where convenient, matrix notation is used. Matrices are denoted by tilde subscripts, such as $\underset{\sim}{n}$. Lower case letters designate column matrices or vectors, whereas upper case letters designate rectangular matrices. The superscript "T" denotes a transpose, as in $\underset{\sim}{n}^T$.

1.2 Mapping, Displacement Field and Fundamental Equations

The mapping between the physical and reference domains of the element, which are shown in Fig. 1, are given by

$$x_i = x_{iI}\, N_I(\xi, \eta, \zeta) \tag{1.2.1}$$

where ξ, η, ζ are the coordinates in the reference cube of dimension 2x2x2 with the origin at the centroid of the element.

The shape functions N_I are given by

$$N_I(\xi, \eta, \zeta) = \frac{1}{8}\,(1 + \xi_I\xi)\,(1 + \eta_I\eta)\,(1 + \zeta_I\zeta_I) \tag{1.2.2}$$

where ξ_I, η_I, ζ_I are the coordinates of node I in the reference domain, which are all $\pm$ 1.

The displacement and velocity fields in the element are given by the same shape functions since the element is isoparametric, hence

$$u_i = u_{iI}\, N_I \tag{1.2.3a}$$

$$v_i = v_{iI}\, N_I \tag{1.2.3b}$$

where u_i and v_i are the displacement and velocity fields and u_{iI} and v_{iI} the components of the nodal displacements and velocities of node I.

The velocity strains are given by

$$\dot{\epsilon}_{ij} = \frac{1}{2}\left(\frac{\partial N_I}{\partial x_j}\, v_{iI} + \frac{\partial N_I}{\partial x_i}\, v_{jI}\right) \tag{1.2.4}$$

and the spin rates by

$$\omega_i = e_{ijk}\, W_{jk} \tag{1.2.5a}$$

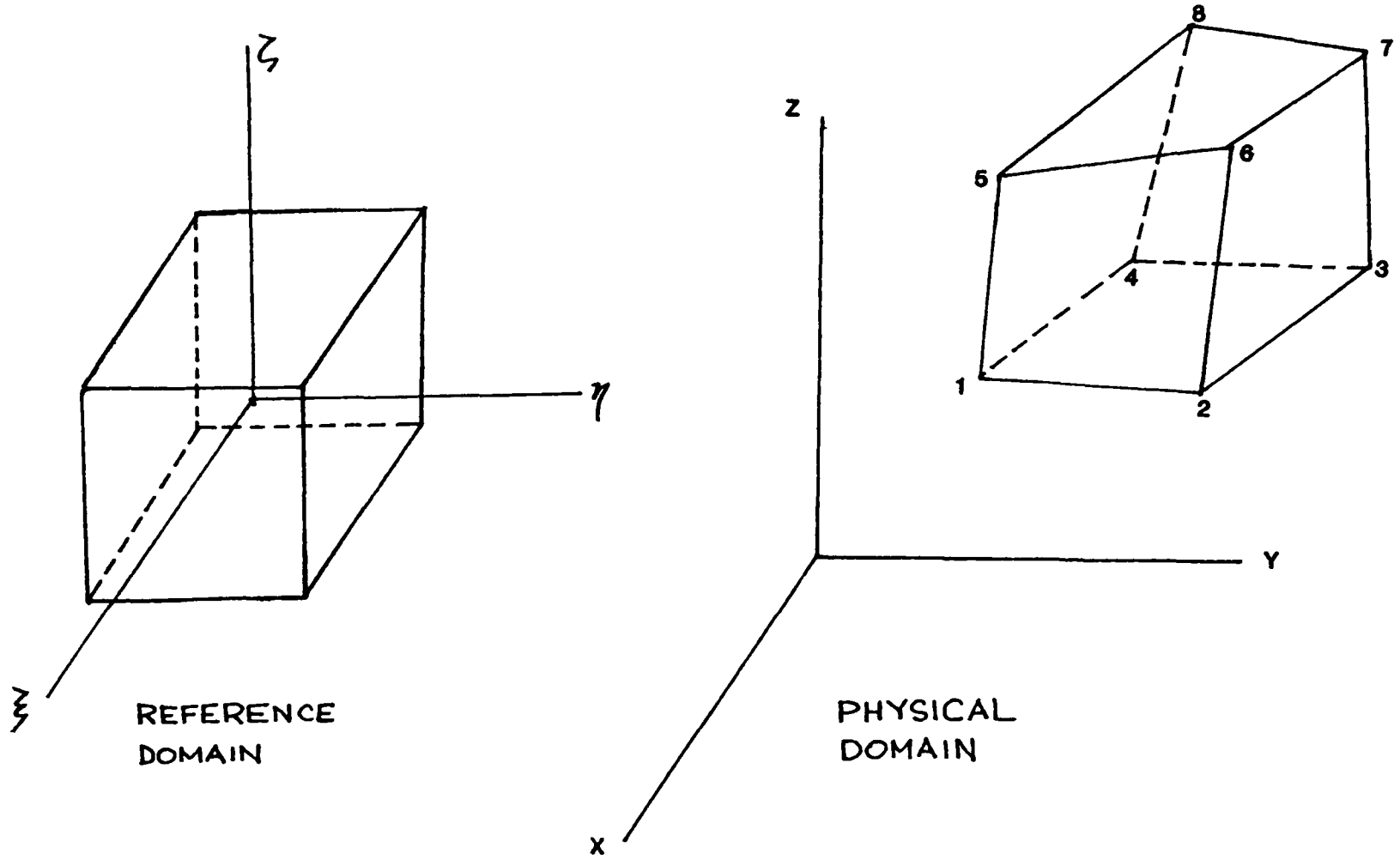

Fig. 1 Element reference and physical domain

$$W_{jk} = \frac{1}{2}\left(\frac{\partial N_I}{\partial x_k} v_{jI} - \frac{\partial N_I}{\partial x_j} v_{kI}\right) . \qquad (1.2.5b)$$

The element nodal forces are given by [2]

$$f_{iI} = \int_{V^e} \frac{\partial N_I}{\partial x_j} \sigma_{ij} \, dV \qquad (1.2.6)$$

where σ_{ij} are the stresses. If we let B_{jI} be an average value of the gradient of shape function matrix, then in one-point quadrature Eq. (2.6) is replaced by

$$f_{iI} = V^e \left(B_{jI} \sigma_{ij} + \gamma_{\alpha I} Q_{\alpha i}\right) . \qquad (1.2.7)$$

Only the first term on the right side of (2.7) originates from (2.6); $Q_{\alpha i}$, $\alpha = 1$ to 4, are the generalized antihourglass stresses and $\gamma_{\alpha I}$ are the hourglass operators which are defined later and must be added to control hourglass modes.

1.3 B - Matrix

Two forms of the $\underset{\sim}{B}$-matrix are incorporated in the program. In the form given in Ref. [2],

$$\bar{B}_{11} = 12VB_{11} = y_2(z_{63} + z_{54}) + y_3 z_{24} + y_4(z_{38} + z_{25})$$
$$+ y_5(z_{86} + z_{42}) + y_6 z_{52} + y_8 z_{45} \qquad (1.3.1a)$$

where

$$x_{IJ} = x_I - x_J, \quad y_{IJ} = y_I - y_J, \quad z_{IJ} = z_I - z_J. \qquad (1.3.1b)$$

The other terms of the $\underset{\sim}{B}$ matrix in row 1 are obtained by simply permuting the nodal coordinates according to Table 1.

where

$$B_1^{(5)} = \frac{1}{12}\left[(2y_5 - y_3)\, z_{42} + y_2\,(z_{53} + z_{54}) + y_4\,(-z_{53} - z_{52})\right]$$

$$B_2^{(5)} = \frac{1}{12}\left[(y_4 - 2y_5)\, z_{31} + y_3\,(z_{54} + z_{51}) + y_1\,(-z_{54} - z_{53})\right]$$

$$B_3^{(5)} = \frac{1}{12}\left[(y_1 - 2y_5)\, z_{42} + y_4\,(z_{51} + z_{52}) + y_2\,(-z_{51} - z_{54})\right]$$

$$B_4^{(5)} = \frac{1}{12}\left[(2y_5 - y_2)\, z_{31} + y_1\,(z_{52} + z_{53}) + y_3\,(-z_{52} - z_{51})\right]$$

$$B_5^{(5)} = \frac{1}{12}\left[(y_{54} - y_{52})z_{31} - (y_{53} - y_{51})z_{42} - (z_{51} - z_{53})y_{42} + (z_{52} - z_{54})y_{31}\right]. \qquad (2.3.5)$$

In using these formulas, nodes 1 to 4 must define a side of an element and must be numbered so that they are counterclockwise when viewed from a point inside the element.

As soon as any volume is found to be negative, the slave node can be considered to definitely lie outside the element. All 6 pentahedral volumes must be positive if the nodes are inside the element.

2.4 Normal Directions

An important ingredient in defining the interaction of the slave nodes and master elements is that any transfer of momentum which occurs between the target and penetrator (other than that due to friction, which is not considered here) should be in directions normal to the interface. For this purpose, the normal vectors must be available when the positions of the slave nodes are adjusted. Since an interaction surface is never defined, it is necessary to construct normals in an alternative manner.

The assembly procedure of the finite element method provides a very natural and concise way of computing these normal vectors. We will first present the procedure in a two dimensional setting so that its ingredients may be understood and visualized more readily and then present the three dimensional equations.

The basic idea of this method is that the normals for each side of the element are computed and added component by component into a normal vector array according to node numbers. The procedure is illustrated in Fig. 6. Note that on interior nodes the assembled normal vectors essentially cancel, so their components are very small or zero. On exterior nodes, the normal vectors point out from the domain with a direction which reasonably approximates a normal to a surface on the edge of the domain. In particular, the normal at a corner takes an average direction of the surfaces that meet at the corner.

In three dimensions, the procedure consists of the following: for each side of the element with local nodes 1, 2, 3, 4, a vector normal to the side is approximately computed by

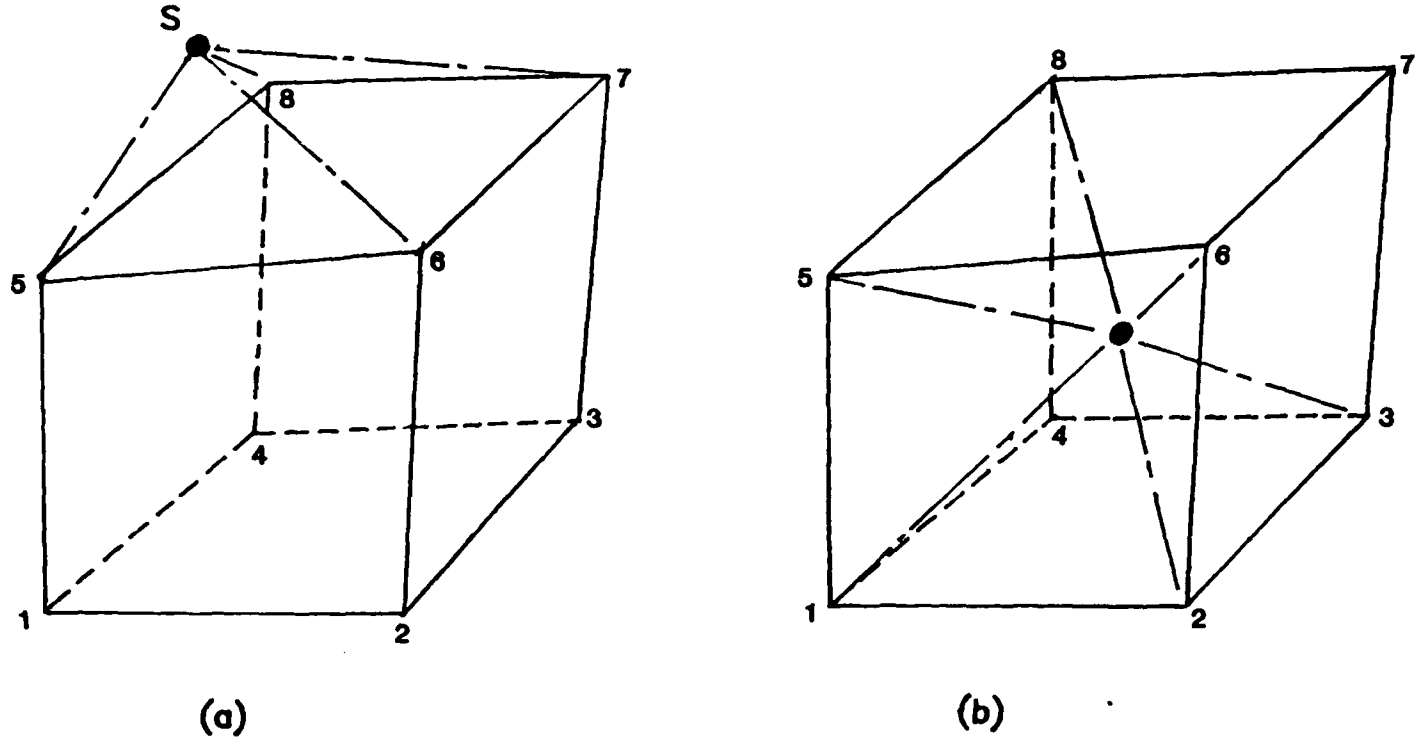

Fig. 5 Penetration check showing the pentahedral volumes which are computed. In (a) the volume 5 - 8 - 6 - 7 - S is negative, in (b) all 6 pentrahedra have positive volumes.

where

$$\| \underset{\sim}{x}_K - \underset{\sim}{x}_J \|^2 = (x_K - x_J)^2 + (y_K - y_J)^2 + (z_K - z_J)^2 \qquad (2.3.3)$$

and where the correspondence between I, J and K is given by

I	K	J
1	7	1
2	8	2
3	6	4
4	3	5

The square of the radius is used in all computations.

All slave nodes which are located in cells which are occupied by nodes of the master element are processed to check whether they are in the element. If an element node occurs in a cell which has a leading zero in LOCSLA, then the cell contains no slave nodes, so no checks need to be made. Otherwise, the process of determining whether a slave node occurs in the element begins. In order to reduce computations, the slave nodes which are sufficiently far from the master element are first eliminated from consideration by the radius check.

If a slave node is within the radius R_e of the master element, the more exact and time consuming checks are made on the slave to see whether it is within the element. If the slave node is within the element, the position of the slave node is adjusted and the corresponding momentum is transferred to the appropriate nodes of the master element. In addition, the slave node number is deleted from the LOCSLA list so that this slave node is not checked against other elements. The details of this are given in Section 2.5.

Once a slave node has passed the simple checks for possible penetration, definitive check is made as to whether the node is within the element. This is accomplished by constructing six pentahedra, each consisting of a side of the hexahedron and the slave node, as shown in Fig. 5. If the volumes of all six pentahedra are positive, the slave node must be within the element.

The volumes of the pentahedra are computed by using Eq. (1.3.4) with nodes 5 to 8 considered coincident. This gives the following formula for the volume of the pentahedra

$$V = \sum_{I=1}^{5} x_I \, B_I^{(5)} \qquad (2.3.4)$$

calculations performed so far. The number of slave nodes per cell is presently limited to 40 but this can easily be increased by changing the dimension of the array LOCSLA, as described later.

2.3 Element Penetration Detection

Any slave nodes which penetrate an element are treated during a loop through the elements; this loop is separate from the element loop in which the nodal forces are updated, and considers only master elements. The element level steps consist of the following for each element e:

1. determine whether any slave node has penetrated element e;
2. if a slave node has penetrated element e, place the node outside the element and transfer the momentum loss to the element nodes.

Note that this procedure is carried out only for master elements so the subdomain of the target that is designated to consist of master elements must be sufficiently large so that no slave node can penetrate the target without penetrating a master element.

The algorithm for step 1 must be streamlined as much as possible in order to insure that computer time is not wasted. The cell scheme is used to minimize as much as possible the number of computations required. The details of the procedure are as follows.

The cell number of each node of the element is determined. As shown in Fig. 4, it is possible for the element to be in several cells. (Note for future work, it may be possible to avoid this by using an overlapping cell lattice so that for any element in the cell, all slave nodes contained in the element must be in the same cell as the centroid of the element.) The cell numbers of the nodes are determined in subroutine LOCNOD, which is the same subroutine that is used for determining the slave node cell location. If ICELL = 0, the node is not in the interaction zone, so it need not be considered. The cell numbers of all nodes of the element are checked against those of the other nodes so that no duplicate cell numbers are considered in checking for slave node penetration of the element.

To determine which slave nodes are in an element, all slaves in the same cell as the element are checked. First a rough check is made. For this purpose, the centroid of the element is defined by

$$\underset{\sim}{x}_c^e = \frac{1}{8} \sum_{I=1} \underset{\sim}{x}_I \qquad (2.3.1)$$

where $\underset{\sim}{x}_I$ are the coordinates of node I. The radius of the element is defined by

$$R_e^2 = \frac{1}{4} \max \| \underset{\sim}{x}_K - \underset{\sim}{x}_J \| \qquad \text{for } I = 1 \text{ to } 4 \qquad (2.3.2)$$

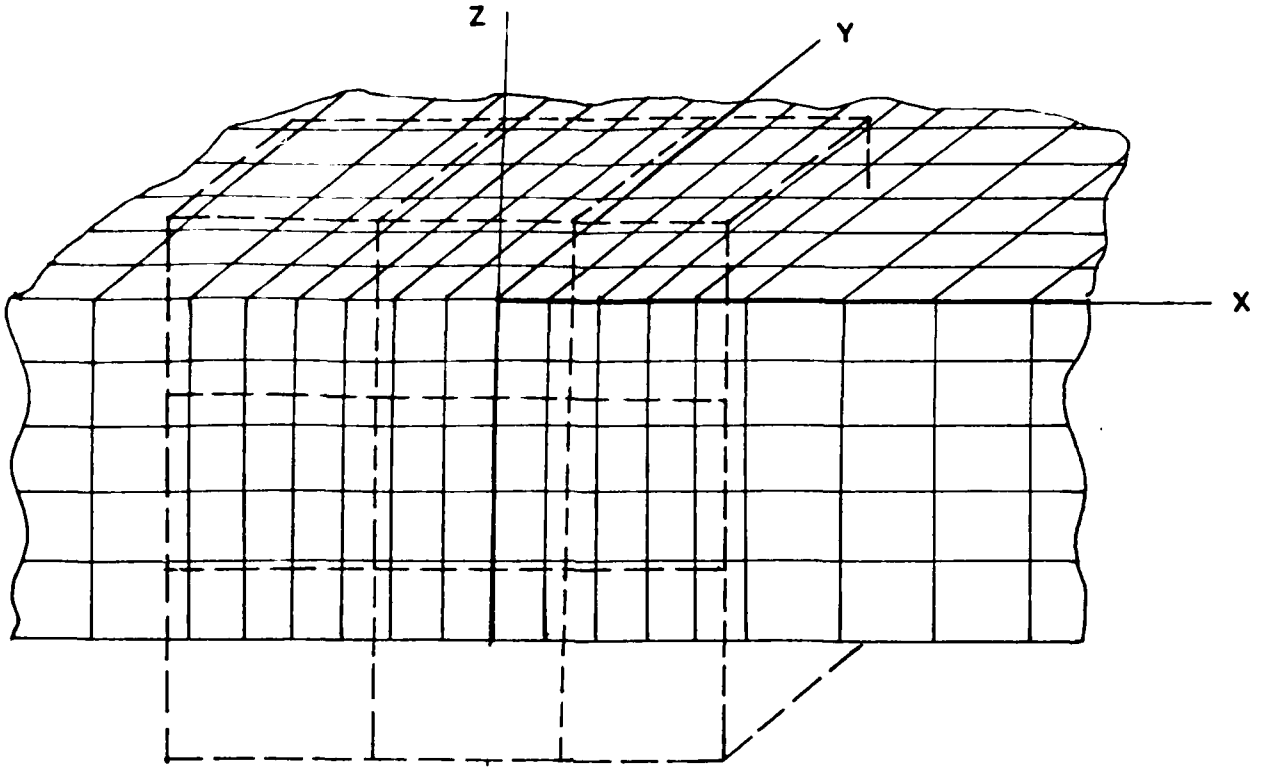

Fig. 3 A 3 x 1 x 3 cell structure.

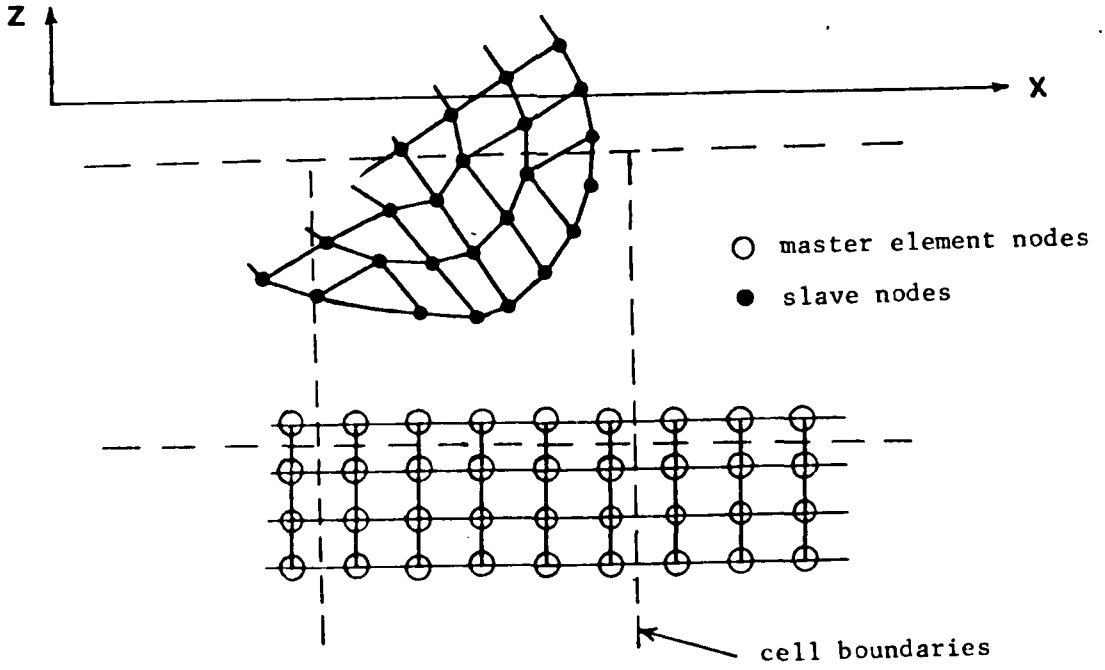

Fig. 4 Two dimensional view of cell structure showing elements in more than one cell.

(y_{min}, y_{max}, NCY) (2.2.2)

(z_{min}, z_{max}, NCZ) (2.2.3)

Here x_{min} and x_{max} are the x-coordinates of the extreme points of the cell domain and NCX is the number of cells in the x-direction; the definitions of the terms in (2.2) and (2.3) are analogous.

The cell location of a node with coordinates (x, y, z) is computed in two steps. First the integer cell numbers in the x, y and z directions are computed by

$$IX = NCX^* (x - x_{min}) / (x_{max} - x_{min}) + 1 \quad (2.2.4a)$$

$$IY = NCY^* (y - y_{min}) / (y_{max} - y_{min}) + 1 \quad (2.2.4b)$$

$$IZ = NCZ^* (z - z_{min}) / (z_{max} - z_{min}) + 1 \quad (2.2.4c)$$

These numbers are then used to compute the cell number of the node, ICELL, as follows. If the node is outside the cell domain, the cell number ICELL is set to zero, i.e.

```
ICELL = 0  if  IX < 1   or   IX > NCX
           or  IY < 1   or   IY > NCY
           or  IZ < 1   or   IZ > NCZ
```
(2.2.5)

Otherwise, ICELL is computed by

```
ICELL = (IZ-1)*NCX*NCY + (IY-1)*NCX + IX
```
(2.2.6)

The locations of all slave nodes are stored in an array K=LOCSLA(IC,J) where IC is the cell number and K is the node number of the J^{th} slave node in cell IC. IF LOCSLA(IC,1)=0, then no slave nodes are located within cell IC.

The identification of the cell locations of slave nodes is made during the time integration loop. As the new positions of slave nodes are calculated (prior to any adjustment for interaction with master elements), the cell number is obtained by the subroutine LOCNOD.

For purposes of efficiency, the cell structure should extend only over the domain in which interaction is expected. This includes the domain occupied by the master elements in the undeformed configuration and any part of the domain into which master elements are anticipated to move as a result of the interaction. Although the optimal relation between cell size and master element size has to be determined, a cell should span at least two element lengths in each direction to reduce the number of elements which occupy more than one cell. A cell structure consisting of 3 x 3 x 1 cells in the x, y and z directions as shown in Fig. 3 has been found quite effective in the

identify all slave nodes in a cell, and then in treating an element to identify the cell number in which it is located and to check the slave nodes which occupy the same cells in the interaction algorithm.

The steps of the interaction procedures within the structure of the complete algorithm is shown in Table 4. As can be seen, the locations of the slave nodes are determined during the time integration of the velocities. Penetration of master elements by slave nodes is then determined in a loop over all master elements. This loop must precede the element loop in which new nodal forces are determined because the interaction algorithm modifies the velocities of the slave nodes and master element nodes.

Table 4

1. initial conditions: velocities and positions of all nodes
2. integrate velocities to obtain new displacements
3.* determine the cell locations of all slave nodes

4.* for each master element:
   - 4. compute surface normal vectors and assemble into global array
   - 4b. determine cells in which element is located
   - 4c. by checking all slave nodes in these cells, determine if any slave nodes are in the element
   - 4d. if a slave node is in the element, move it back to an outside surface and transfer the momentum to the element nodes, which modifies its nodal velocities

5. for each element:
   - 5a. compute strain-rates from the nodal velocities and stress-rates from the constitutive equations
   - 5b. integrate stress-rates to obtain new stresses and compute nodal forces
   - 5c. assemble nodal forces into global array

6. find nodal accelerations from equations of motion
7. integrate accelerations to find new velocities; go to 2

* denotes steps which pertain to the interaction algorithm

2.2 Cell Structure and Location of Nodes

The cell structure which is used to identify the slave nodes and master elements for which interaction is possible is shown in Fig. 3. The cells are uniform in size in all directions and their edges are parallel to the x, y and z coordinates.

The cell domain is described by the following:

$$(x_{min}, x_{max}, NCX) \qquad (2.2.1)$$

Section 2

INTERACTION ALGORITHMS

2.1 Overview

The basic purpose of this algorithm is to treat the interaction of two bodies with eroding elements. Eroding elements are elements which are destroyed during the course of the computation because of very high strains, which implies that they represent elements of the target or penetrator which have ceased to play a significant role in the physics of the problem.

Algorithms with eroding elements in three dimensions are very difficult to treat within the conventional framework of master and slave contact surfaces. It is difficult to design algorithms to redefine the contact surfaces when elements are destroyed, particularly in three dimensions. Moreover, the corners which are created in the surfaces by the erosion of elements present severe algorithmic difficulties.

Therefore, this new algorithm uses a concept of slave nodes and master elements. One of the two bodies, usually the projectile, is defined by the nodes, hereafter called slave nodes; the second body is defined by elements, called master elements. If a slave node is found to be inside a master element, it is then brought back to an outside surface. In order to determine the outside surfaces, a set of normal vectors is assembled for all master elements as described in Section 2.4. Because of the character of the assembly process, a nonzero normal vector will only result on outside surfaces and will provide an effective average normal to the surface.

The mechanics of the interaction of the two bodies is executed completely through the interaction of the slave nodes with the master elements. The rules of this interaction are as follows:

i) Slave nodes are not permitted to penetrate master elements.
ii) Whenever penetration of a slave node into a master element is detected, the slave node is returned to the surface of the element it has penetrated and the associated loss of momentum is transferred to the appropriate nodes of the master element. If a check on nodal normals shows that this is not an exterior surface, the node is moved to the appropriate edge.

The efficacy of this procedure hinges strongly on the use of explicit time integration, since stability requirements then limit the time step so that the master element which is penetrated effectively represents the zone of the interaction. Because of the large number of slave nodes and master elements involved in this process, special techniques are needed to quickly identify the slave nodes and master elements between which interaction is possible. This is accomplished by using a cell structure which is fixed in space. Cells are considered to be substantially larger than elements and so may include many master elements and slave nodes. The basis of the procedure is to

$$\Delta t = \frac{2}{\omega}\left[(1 + \xi^2)^{1/2} - \xi\right] \qquad (1.6.2)$$

where ξ is the fraction of critical damping in the maximum frequency. This time step is always smaller than the stable time step for linear problems.

$$\gamma_{\alpha I} = h_{\alpha I} - (h_{\alpha J}\, x_{jJ})\, B_{jI} \,. \tag{1.5.2}$$

In the above, the vectors $\underset{\sim}{h}_\alpha$ are defined in Table 3.

Table 3. The $\underset{\sim}{h}_\alpha$ and $\underset{\sim}{s}$ vectors for the hexahedron

I =	1	2	3	4	5	6	7	8
h_{1I}	+1	+1	-1	-1	-1	-1	+1	+1
h_{2I}	+1	-1	-1	+1	-1	+1	+1	-1
h_{3I}	+1	-1	+1	-1	+1	-1	+1	-1
h_{4I}	-1	+1	-1	+1	+1	-1	+1	-1
Λ_{1I}	-1	+1	+1	-1	-1	+1	+1	-1
Λ_{2I}	-1	-1	+1	+1	-1	-1	+1	+1
Λ_{3I}	-1	-1	-1	-1	+1	+1	+1	+1

The hourglass strain-rates give the rates of the generalized hourglass stresses

$$\overset{\nabla}{Q}_{i\alpha} = G_{ij}\, \dot{q}_{j\alpha} \tag{1.5.3}$$

where the rate of $Q_{i\alpha}$ is related to its frame-invariant rate of $\overset{\nabla}{Q}_{i\alpha}$ by

$$\dot{Q}_{i\alpha} = \overset{\nabla}{Q}_{i\alpha} + W_{ij}\, Q_{j\alpha} \tag{1.5.4}$$

The constants G_{ij} are given by

$$G_{ij} = \varepsilon\, \bar{\omega}\, \delta_{ij} \tag{1.5.5}$$

where $\bar{\omega}$ is an estimate of the maximum frequency and ε a user-controlled parameter. Values of 0.03 to 0.10 are recommended for ε.

1.6 Element Frequency and Stable Time Step

The stable time step for the element is computed by using the following upper bound for the maximum element frequency taken from Ref. [4]

$$\omega^2_{max} \leq \bar{\omega}^2 = 8c^2\, B_{iI}\, B_{iI} \tag{1.6.1}$$

where c is the dilatational wavespeed. The time step computed by

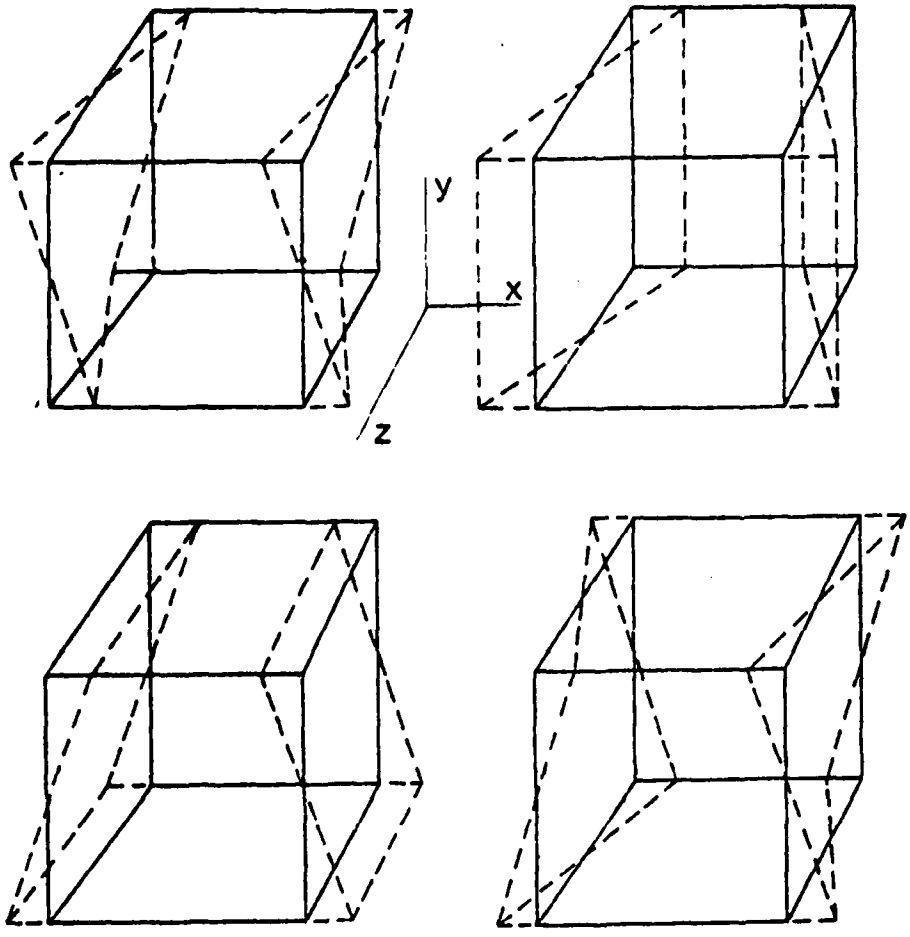

Fig. 2 Hourglass modes involving x-component, u_x

The advantage of this form over Eq. (3.1) is apparent in Eq. (3.6), which shows that the last four terms of B_{iI} need not be computed. On the other hand, Eq. (3.1) applies to degenerate hexahedra such as tetrahedra, whereas Eq. (3.5) does not.

1.4 Stress-Strain Relationship

The element can use any nonlinear stress-strain law, but for an anisotropic stress-strain law the material matrices must be updated as indicated in Ref. [5], which is indicated by Eq. (1.4.4). The measure of stress in this element is the Cauchy stress, or physical stress, and the measure of deformation is the velocity strain, also known as rate-of-deformation. This will usually be called the strain-rate. In order to maintain frame-invariance in a stress-strain law based on these measures, a frame-invariant stress rate must be used. Here, the Jaumann rate is used. If the material stress rate is related to the strain rate by

$$\overset{\nabla}{\sigma}_{ij} = C_{ijk\ell}\,\dot{\varepsilon}_{k\ell} \tag{1.4.1}$$

then the rate of change of the stress is given by

$$\dot{\sigma}_{ij} = \overset{\nabla}{\sigma}_{ij} + W_{ik}\,\sigma_{kj} + W_{jk}\,\sigma_{ki}\ . \tag{1.4.2}$$

For any isotropic material, Eq. (4.1) can be written as

$$\overset{\nabla}{\sigma}_{ij} = \lambda\,\dot{\varepsilon}_{kk}\,\delta_{ij} + 2\mu\,\dot{\varepsilon}_{ij} \tag{1.4.3}$$

where λ and μ are the Lame constants.

This form of the stress-strain relations is frame-invariant only if the material is and remains isotropic. For anisotropic materials, the $\underset{\sim}{C}$ matrix must be updated as follows [5]

$$\dot{C}_{ijk\ell} = \overset{\nabla}{C}_{ijk\ell} + W_{ia}\,C_{ajk\ell} + W_{jb}\,C_{ibk\ell} + W_{kc}\,C_{ijc\ell} + W_{\ell d}\,C_{ijkd}\ . \tag{1.4.4}$$

1.5 Hourglass Control

When the nodal forces of the hexahedron are evaluated by one-point quadrature, it possesses 12 spurious zero-energy modes or hourglass modes. The modes occur independently in the x, y and z directions. The four modes in the x-direction are shown in Fig. 2; the modes in the y and z directions can be envisioned by simply replacing the x-axis by the y or z axes.

To control these modes, 12 additional generalized strain-rates are defined by

$$\dot{q}_{i\alpha} = \gamma_{\alpha I}\,v_{iI} \tag{1.5.1}$$

where the range of Greek letters is 4, and

In the centroidal form, the $\underset{\sim}{B}$ matrix is evaluated at the centroid of the element, that is, the point $\xi = \eta = \zeta = 0$. In this form, the $\underset{\sim}{B}$ matrix is given by

$$B_{x1} = \frac{1}{J_o}\left[(z_{54} + z_{63})\, y_{28} + (z_{42} + z_{86})\, y_{53} + (z_{52} + z_{83})\, y_{64}\right]$$

$$B_{x2} = \frac{1}{J_o}\left[(z_{63} + z_{54})\, y_{71} - (z_{61} + z_{74})\, y_{53} - (z_{31} + z_{75})\, y_{64}\right]$$

$$B_{x3} = \frac{1}{J_o}\left[-(z_{42} + z_{86})\, y_{71} - (z_{74} + z_{61})\, y_{28} - (z_{72} + z_{81})\, y_{64}\right]$$

$$B_{x4} = \frac{1}{J_o}\left[-(z_{83} + z_{52})\, y_{71} - (z_{31} + z_{75})\, y_{28} + (z_{81} + z_{72})\, y_{53}\right] \qquad (1.3.5)$$

where J_o is the Jacobian at the centroid. The terms B_{x5} to B_{x8} are then obtained by

$$\begin{aligned} B_{x5} &= -B_{x3} \\ B_{x6} &= -B_{x4} \\ B_{x7} &= -B_{x1} \\ B_{x8} &= -B_{x2} \end{aligned} \qquad (1.3.6)$$

The terms of $\underset{\sim}{B}$ associated with y and z, i.e. the second and third rows, are obtained by the same permutations of x, y, and z on the right hand side as indicated in Table 2.

The Jacobian is given by

$$J_o = \det \begin{bmatrix} x_{,\xi} & y_{,\xi} & z_{,\xi} \\ x_{,\eta} & y_{,\eta} & z_{,\eta} \\ x_{,\zeta} & y_{,\zeta} & z_{,\zeta} \end{bmatrix} \qquad (1.3.7)$$

where

$$x_{i,\xi} = \frac{1}{8}\Lambda_{1I}\, x_{iI} \qquad (1.3.8a)$$

$$x_{i,\eta} = \frac{1}{8}\Lambda_{2I}\, x_{iI} \qquad (1.3.8b)$$

$$x_{i,\zeta} = \frac{1}{8}\Lambda_{3I}\, x_{iI} \qquad (1.3.8c)$$

and Λ_{iI} are given in Table 3.

Table 1. Permutations of node numbers for generating B_{1I} from B_{11}

1	2	3	4	5	6	7	8
2	3	4	1	6	7	8	5
3	4	1	2	7	8	5	6
4	1	2	3	8	5	6	7
5	8	7	6	1	4	3	2
6	5	8	7	2	1	4	3
7	6	5	8	3	2	1	4
8	7	6	5	4	3	2	1

For example

$$12V\ B_{13} = y_4(z_{81} + z_{72}) + y_1\ z_{42} + y_2(z_{16} + z_{47}) + y_7(z_{68} + z_{24}) + y_8\ z_{74} + y_6\ z_{27}\ . \tag{1.3.2}$$

The other three rows are obtained by interchanging x, y, z according to Table 2.

Table 2. Permutations of coordinates for generating rows 2 and 3 from row 1

Row		
1	y	z
2	z	x
3	x	y

For example

$$12V\ B_{33} = \left[x_4\ (y_{81} + y_{72}) + x_1\ y_{42} + x_2(y_{16} + y_{47}) + x_7(y_{68} + y_{24}) + x_8\ y_{74} + x_6\ y_{27}\right]. \tag{1.3.3}$$

The volume of the element is obtained by

$$V = \frac{1}{12}\ \overline{B}_{1I}\ x_{1I} = \frac{1}{12}\ \overline{B}_{2I}\ x_{2I} = \frac{1}{12}\ \overline{B}_{3I}\ x_{3I}\ . \tag{1.3.4}$$

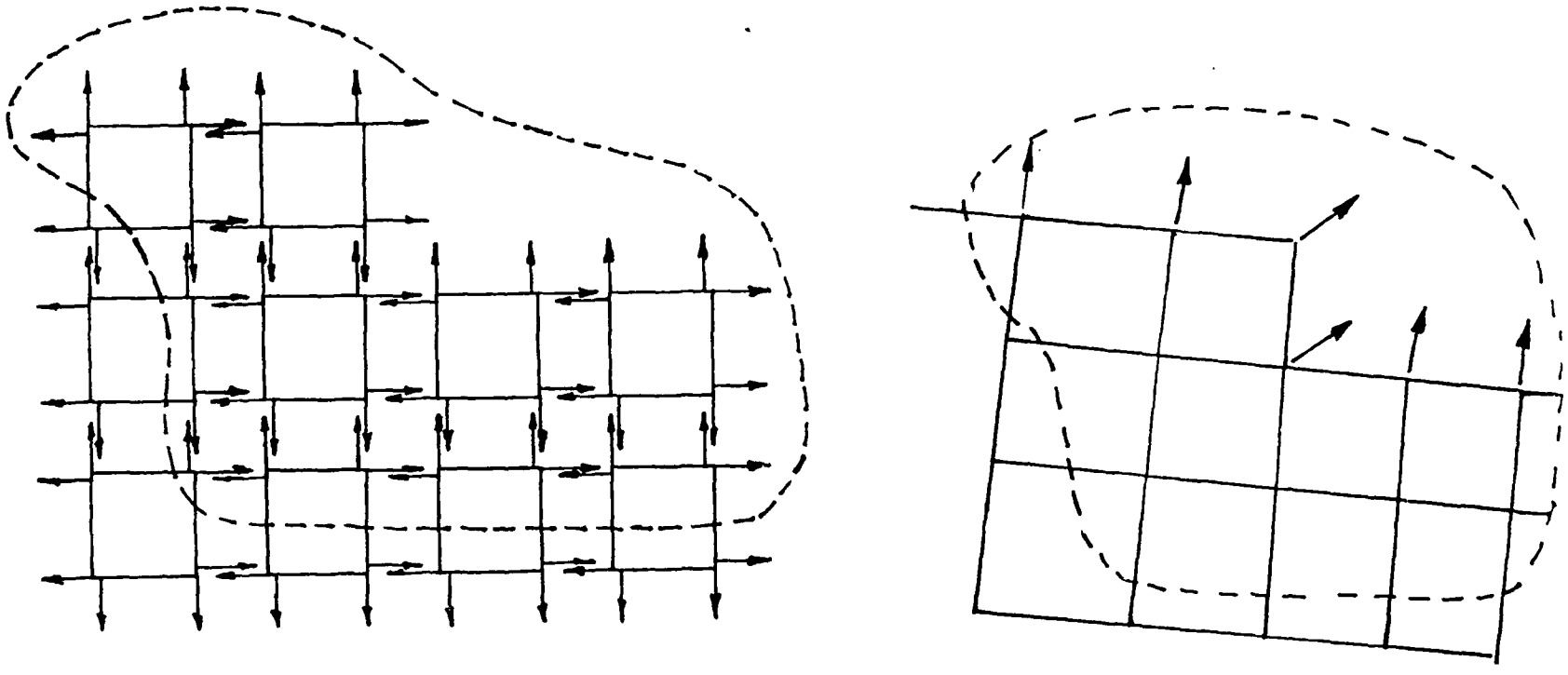

Fig. 6 Assembly of normals from master elements to determine outside surfaces; only elements within dashed contour are considered.

$$\underset{\sim}{n} = \underset{\sim}{x}_{42} \times \underset{\sim}{x}_{31} \qquad (2.4.1)$$

where (x) designates a vector cross-product. This vector $\underset{\sim}{n}$ is normalized and then assembled into the global arrays of the normals of 4 nodes by adding each component of the vector $\underset{\sim}{n}$ to the existing vector in the nodal array. When the contribution of each element has been added to the nodal arrays, the procedure is complete. The procedure can be summarized as follows:

1. Initialization at beginning of time step: zero the vectors $\underset{\sim}{n}_I$ for all nodes I.

2. For each element e in the set of master elements:
   2.1 For each side of the element, compute $\underset{\sim}{n}$;
   2.2 add $\underset{\sim}{n}$ into the arrays $\underset{\sim}{n}_I$ of the four nodes which define the side.

Remarks:

1. In order to avoid difficulties with master elements at the edge of the master element domain, the master elements should be defined, to extend sufficiently far so that the edge master elements are not penetrated from the sides.
2. For nodes of master elements which lie on a plane of symmetry, the components of the normal vector which do not lie in the plane of symmetry are set to zero.
3. For master elements which lie on the bottom of the target (opposite to the original position of the projectile), the normals to the bottom surface are omitted to avoid driving the slave nodes in the wrong direction.

2.5 Adjustment of Slave Node Positions

Once it is determined that a slave node has penetrated a master element, it is necessary to adjust its position consistent with the fact that its normal momentum has been transferred to the target. This procedure involves two steps:

1. using the normal vectors associated with the element, determine in which direction the position of the slave node has to be adjusted;
2. displace the slave node to an outside surface in the direction of the normal $\underset{\sim}{n}$;
3. if the surface to which a slave node is brought is not an outside surface, bring the slave node back to an edge of the surface.

The procedure is implemented as follows. The average normal of the element is found by

$$\bar{\underset{\sim}{n}} = \left(\sum_{I=1}^{8} \underset{\sim}{n}_I \right) / \| \quad \| \qquad (2.5.1)$$

where the division by "‖ ‖" designates normalization of the vector, the norm is defined in Eq. (3.3).Let the current coordinates of the slave node be $\underset{\sim}{x}_o$.

Then the node is displaced by the procedure

$$\underset{\sim}{x}_n = \underset{\sim}{x}_o + \eta\, \bar{\underset{\sim}{n}} \qquad (2.5.2)$$

where η is an undetermined parameter $\eta > 0$.

The magnitude of η is determined by checking which of the sides of the hexahedron is intersected by the line of Eq.(2.5.2). This is accomplished as follows. Each side is subdivided into 2 triangular surfaces (note that this is only an approximation to the surface of an isoparametric hexahedron but it simplifies computations enormously). By taking 3 nodes of the surface in turn, the surface is defined by

$$x_i = x_{iI}\, \xi_I \qquad I = 1 \text{ to } 3 \qquad (2.5.3)$$

$$\xi_1 + \xi_2 + \xi_3 = 1 \; . \qquad (2.5.4)$$

The intersection of the line defined by Eq. (5.2) and the plane is determined by solving the 4 equations in 4 unknowns represented by Eqs. (5.3) to (5.4). The solution is given by

$$\eta = \frac{-1}{D} \det \begin{bmatrix} x_{13} & x_{23} & x_{03} \\ y_{13} & y_{23} & y_{03} \\ z_{13} & z_{23} & z_{03} \end{bmatrix} \qquad (2.5.5a)$$

$$\xi_1 = \frac{1}{D} \det \begin{bmatrix} x_{03} & x_{23} & \bar{n}_x \\ y_{03} & y_{23} & \bar{n}_y \\ z_{03} & z_{23} & \bar{n}_z \end{bmatrix} \qquad (2.5.5b)$$

$$\xi_2 = \frac{1}{D} \det \begin{bmatrix} x_{13} & x_{03} & \bar{n}_x \\ y_{13} & y_{03} & \bar{n}_y \\ z_{13} & z_{03} & \bar{n}_z \end{bmatrix} \qquad (2.5.5c)$$

$$\xi_3 = 1 - \xi_1 - \xi_2 \qquad (2.5.5d)$$

where

$$D = \begin{vmatrix} x_{13} & x_{23} & \bar{n}_x \\ y_{13} & y_{23} & \bar{n}_y \\ z_{13} & z_{23} & \bar{n}_z \end{vmatrix} . \qquad (2.5.6)$$

A particular triangular surface is intersected by the parametric ray of Eq. (5.2) if and only if

$$\eta > 0 \qquad (2.5.7)$$

$$0 \leq \xi_I \leq 1 \quad \text{for} \quad I = 1 \text{ to } 3 , \qquad (2.5.8)$$

Once the surface on which the slave node is projected is determined, the surface is checked to ascertain whether it is an outside surface. This is done by checking whether the 4 normals of the nodes of the surface are non zero. If this check fails, the node is projected to an edge of the surface as shown in Fig. 7.

The equations which govern this realignment of the slave node are the following. Let $\underset{\sim}{x}_n$ be given by

$$\underset{\sim}{x}_n = \underset{\sim}{x}_o + \Delta t \, \underset{\sim}{v}^{old} \qquad (2.5.9)$$

where $\underset{\sim}{x}_o$ is the position of the slave node at the beginning of the time step as shown in Fig. 7. The edges of the side are then considered in turn and its nodes are generically identified as 1 and 2, with the vector connecting them denoted by $\underset{\sim}{x}_{21}$. The previously computed new position of the node is denoted by $\underset{\sim}{x}_m$ where

$$\underset{\sim}{x}_m = \underset{\sim}{x}_n + \Delta \underset{\sim}{r} . \qquad (2.5.10)$$

The node is then repositioned on the intersection of the line $\underset{\sim}{x}_{mo}$ with plane defined by the vectors $\underset{\sim}{x}_m$ and $\underset{\sim}{x}_n$. The equations to be solved are

$$\underset{\sim}{x}_{10} + \underset{\sim}{x}_{21} \xi_1 - \underset{\sim}{x}_{on} \xi_2 - \underset{\sim}{x}_{mn} \xi_3 = 0 \qquad (2.5.11)$$

where ξ_i, $i = 1$ to 3, are the unknowns. If the edge $\underset{\sim}{x}_{21}$ is the correct one ξ_1 must satisfy $0 \leq \xi_1 \leq 1$. Otherwise, another edge of the surface is considered.

The final position is denoted by $\underset{\sim}{x}_f$ which is given by

$$\underset{\sim}{x}_f = \underset{\sim}{x}_1 + \xi_1 \underset{\sim}{x}_{21} \qquad (2.5.12a)$$

where ξ_1 is the above solution. The reposition vector is then redefined by

$$\Delta \underset{\sim}{r} = \underset{\sim}{x}_{fn} = \underset{\sim}{x}_f - \underset{\sim}{x}_n . \qquad (2.5.12b)$$

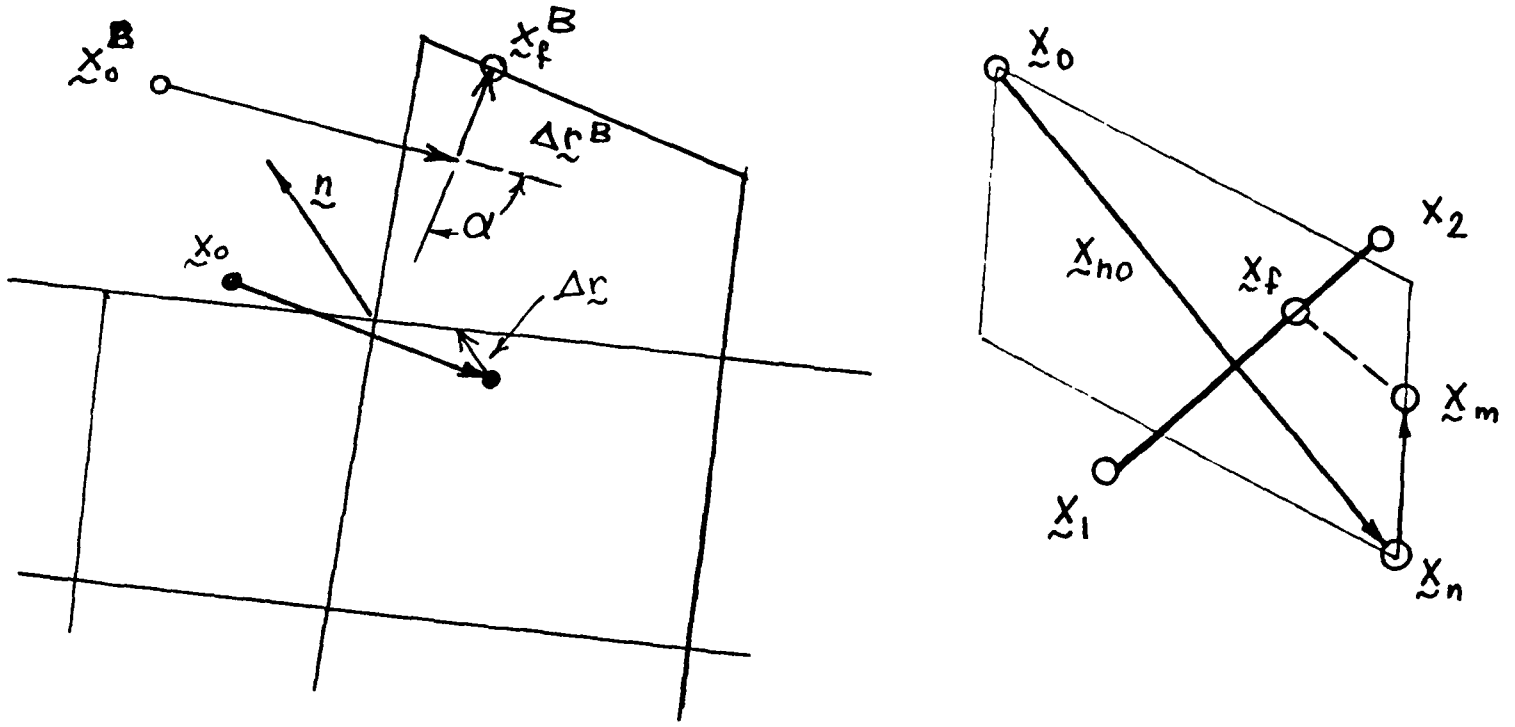

Fig. 7 Procedure for repositioning a slave node when the normal projection leaves it inside the target; node B illustrates a case where velocity is increased by original repositioning.

If a slave node is on a plane of symmetry, the component normal of $\Delta\underset{\sim}{r}$ to the plane of symmetry is now set to zero.

One situation which can foil even this check and allow a slave node to remain within the target is shown in Fig. 8. Here the slave node has penetrated element with nodes numbered 1 to 8. The repositioning will place the node on the surface defined by nodes 1 to 4, and because a single intact element, defined by nodes 1 to 4 and 9 to 12 lies above the intact plane, the normals will be nonzero on each of the four nodes, 1 to 4. Therefore, the node will remain on this surface. However, if all projectile nodes are slave nodes, a subsequent slave node should engage the element defined by nodes 1 to 4 and 9 to 12.

Once the new position of the slave node is determined the change in its velocity is computed by

$$\Delta\underset{\sim}{v} = \Delta\underset{\sim}{r}/\Delta t \tag{2.5.13a}$$

where $\Delta\underset{\sim}{r}$ is the total displacement of the slave node needed. The velocity of the slave node is then modified by

$$\underset{\sim}{v}^{new} = \underset{\sim}{v}^{old} + \Delta\underset{\sim}{v} \ . \tag{2.5.13b}$$

In unusual circumstances it is possible for the normal of an element to form an angle of more than 90^0 with the slave node velocity. This situation is illustrated in Fig. 8, for node B, where α is the angle between the velocity vector and the normal. If the previously described procedures are used, the repositioning of the slave node will increase its velocity and its kinetic energy as shown; note the new velocity vector is longer than the original velocity vector. This repositioning is of course completely contrary to physical laws, since it increases the kinetic energy of the system.

In order to avoid this, the new velocity $\underset{\sim}{v}^{new}$ is compared with the original velocity, $\underset{\sim}{v}^{old}$. It is required that the following inequality be satisfied by these velocities

$$\| \ v^{new} \ \| \leq \| \ \underset{\sim}{v}^{old} \ \| \ . \tag{2.5.14}$$

If this is not satisfied, the node is moved back along the vector $\underset{\sim}{v}^{new}$ until its velocity satisfies the following equation

$$\| \ \underset{\sim}{v}^{new} \ \|^2 \ + \| \ \Delta \ \underset{\sim}{r}/\Delta t \ \|^2 \ = \| \ \underset{\sim}{v}^{old} \ \|^2 \ . \tag{2.5.15}$$

This implies that the angle between $\Delta \ \underset{\sim}{r}$ and $\underset{\sim}{v}^{new}$ will be a right angle. Although this procedure will usually position the slave node outside of the target, it insures that energy is not generated by the procedure. In subsequent time steps the slave node will again penetrate a master element so the procedure is not harmful.

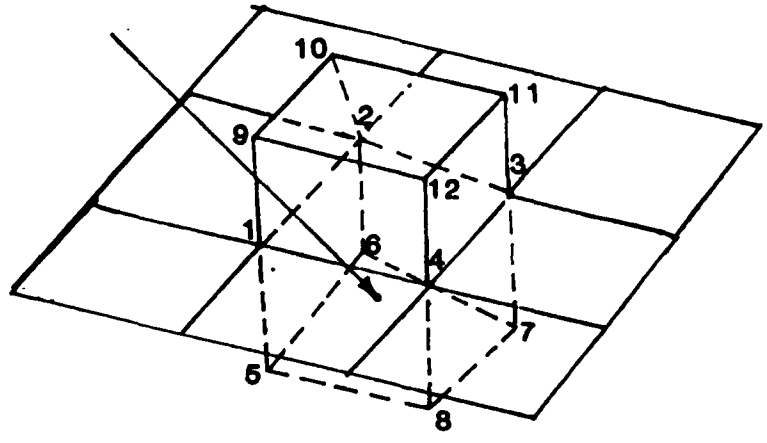

Fig. 8 Depiction of a situation where checking for nonzero normals is not sufficient to detect an interior surface.

The momentum loss associated with this adjustment is $M\Delta\underset{\sim}{v}$, where M is the mass of the slave node. This mass is now transferred to the nodes in contact with the 2 triangles on the penetrated side. The formula used is

$$\Delta v_J = \frac{-M}{rM_J} \underset{\sim}{n}_J^T \bar{\underset{\sim}{n}} \Delta\underset{\sim}{v} \qquad \text{(no sum on J)} \tag{2.5.16}$$

where

$$r = \sum_{I=1}^{4} \underset{\sim}{n}_I^T \bar{\underset{\sim}{n}} \tag{2.5.17}$$

This formula apportions the momentum to the nodes according to how strongly their vectors point in the direction of the interface normal $\bar{\underset{\sim}{n}}$.

Section 3

NUMERICAL EXAMPLES

The sample problems include a very simple, small problem which can be used to quickly check the performance of the program in a new installation and a moderate size problem and large scale problem. In each case, a table of key problem parameters, a printout of the card images of the input data deck and some computer graphics of the evolution of the response are given. The execution speed of the program is 100 elements per time step per CPU second on a CYBER 170/730, 1000 elements per time step on a CDC 7600.

Example 1

The first example involves a simple copper projectile consisting of 24 elements striking a target modeled by 48 elements. The material properties and dimensions are given in Table 5. The evolution of the problem is shown in Fig. 9. As can be seen from Fig. 9, because of the small size of the target, although erosion commences, subsequent momentum transfer causes the target to move away from the projectile.

Example 2

The second example is a problem of moderate scale, involving 88 elements in the projectile and 500 elements in the target. Table 6 gives the problem parameters and card images of the data. The evolution of the problem is shown in Fig. 10. Erosion is only evident in the projectile for the first 77 time steps (cycles) which were run.

Example 3

Example 3 is taken from Ref. [7]. It consists of a copper rod striking a steel plate at 2000 meter/second. The projectile is modeled with 414 elements, the target with 1014 elements. The copper is assigned a failure strain of $\bar{\varepsilon}_p = 2.0$. A complete listing of material and problem parameters is given in Table 7. Note that arbitrary erosion can occur in both the target and projectile.

The simulation is shown in Fig. 11. Note that the projectile starts jetting in the positive x-direction early in the simulation. These large shears result in rapid erosion of the projectile. Subsequently, large deformations in the target result in shear failure in the target. Erosion takes place in both the target and projectile.

In Fig. 11, gaps often appear to develop between the target and projectile. This is partially a result of the use of a two dimensional plot of the plane of symmetry, which cannot show the contact between the projectile and target away from the plane of symmetry.

TABLE 5

Parameters and input for Example 1

Projectile

shape	:	rod
dimensions	:	3 in long, radius 0.6 in
density	:	0.000831 lb-sec^2/in^4
bulk modulus	:	20,739,000 psi
shear modulus	:	6,380,000 psi
yield stress	:	20,300 psi
ultimate stress	:	65,300 psi
initial velocity	:	x-component - 2588.0 in/sec z-component - 9659.0 in/sec

Target

shape	:	plate
dimensions	:	6 in x 3 in x 0.5 in (half plate)
density	:	0.0005 lb-sec^2/in^4
bulk modulus	:	24,200,000 psi
shear modulus	:	9,300,00 psi
yield stress	:	160,000 psi
ultimate stress	:	160,100 psi
initial velocity	:	0

Table 5 Continued

```
l     1     1
l     1    PROJECTILE MATERIAL
,00073   410000.0 23810000.
30000.    250000.    310000.          0.3   9999999.          0.0          1.0
  999.       999.         2.0          0.0
?     1   TARGET MATERIAL
,00073   410000.0 27780000.
50000.    160000.    185000.          0.3   9999999.                       1.0
  999.       999.         0.1          0.0

   1.0        1.0         1.0          0.0         0.2         15.0         0.0
?
?     0     4     0          3.0          0.0         1.0
   0.6        0.0         0.6          0.0

   1.0        1.0         1.0
4     1
?     4     3     3     4     1          1.2         0.3          1.2          1.0 1.
  -3.0        0.0         0.0          3.0         3.0         -0.5

?
?     1     3     1     0     1     0

4     1
8     3     2    61           2     1     1     8     3     1

l     3     1    61     1    60    60     0                      0.0          1.0 1.
?     4     1     9     1


5782.5         0.0  -62633.1                                              0.000001
```

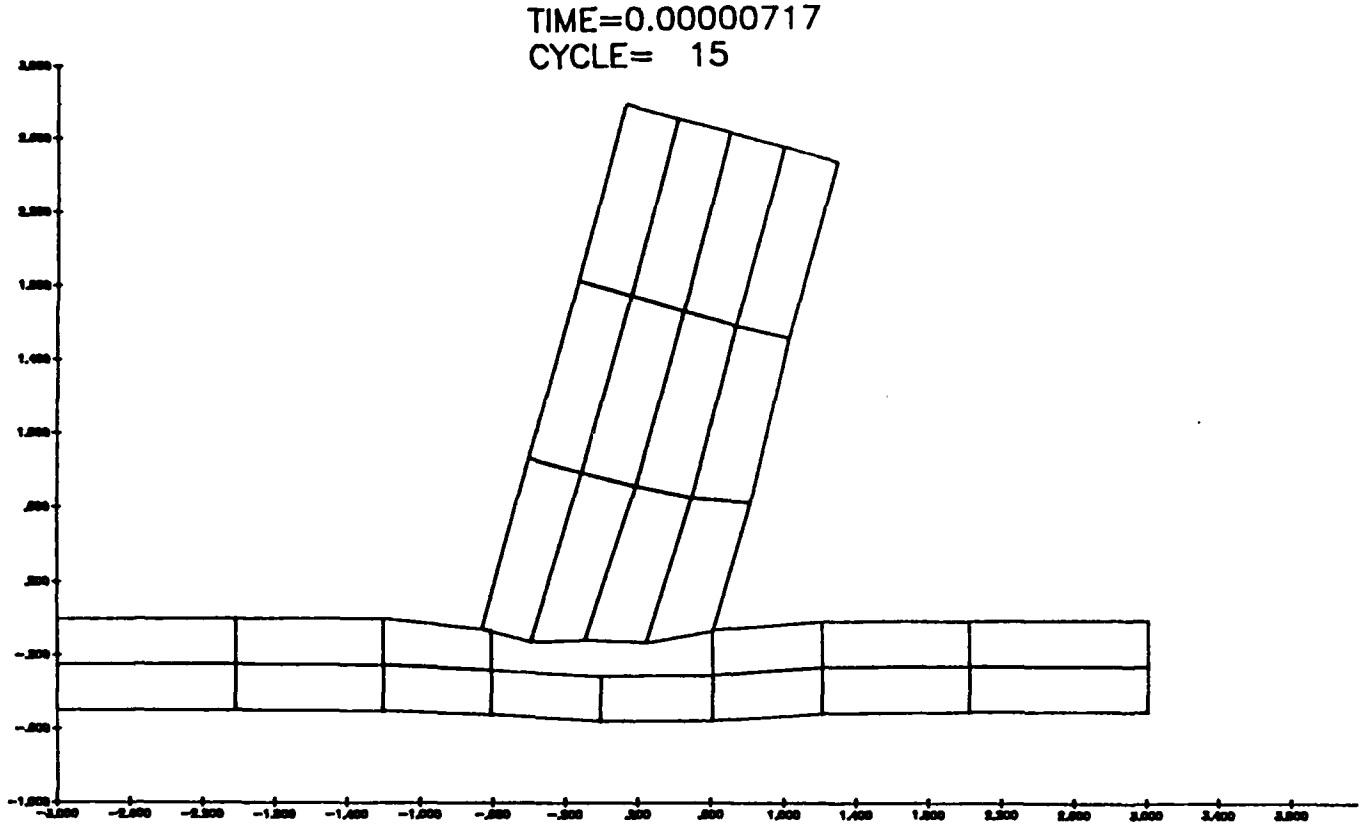

Fig. 9a Evolution of mesh for example 1

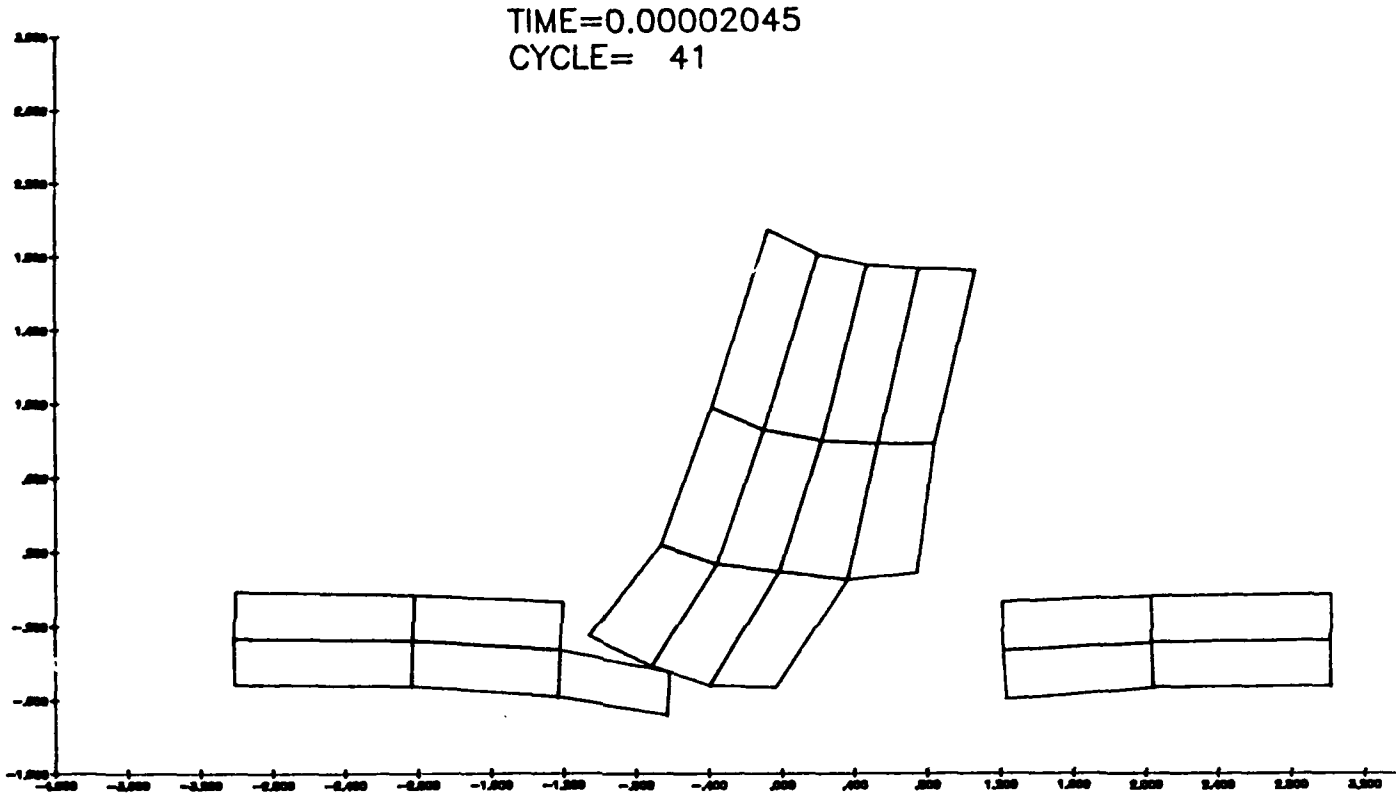

Fig. 9b Evolution of mesh for example 1

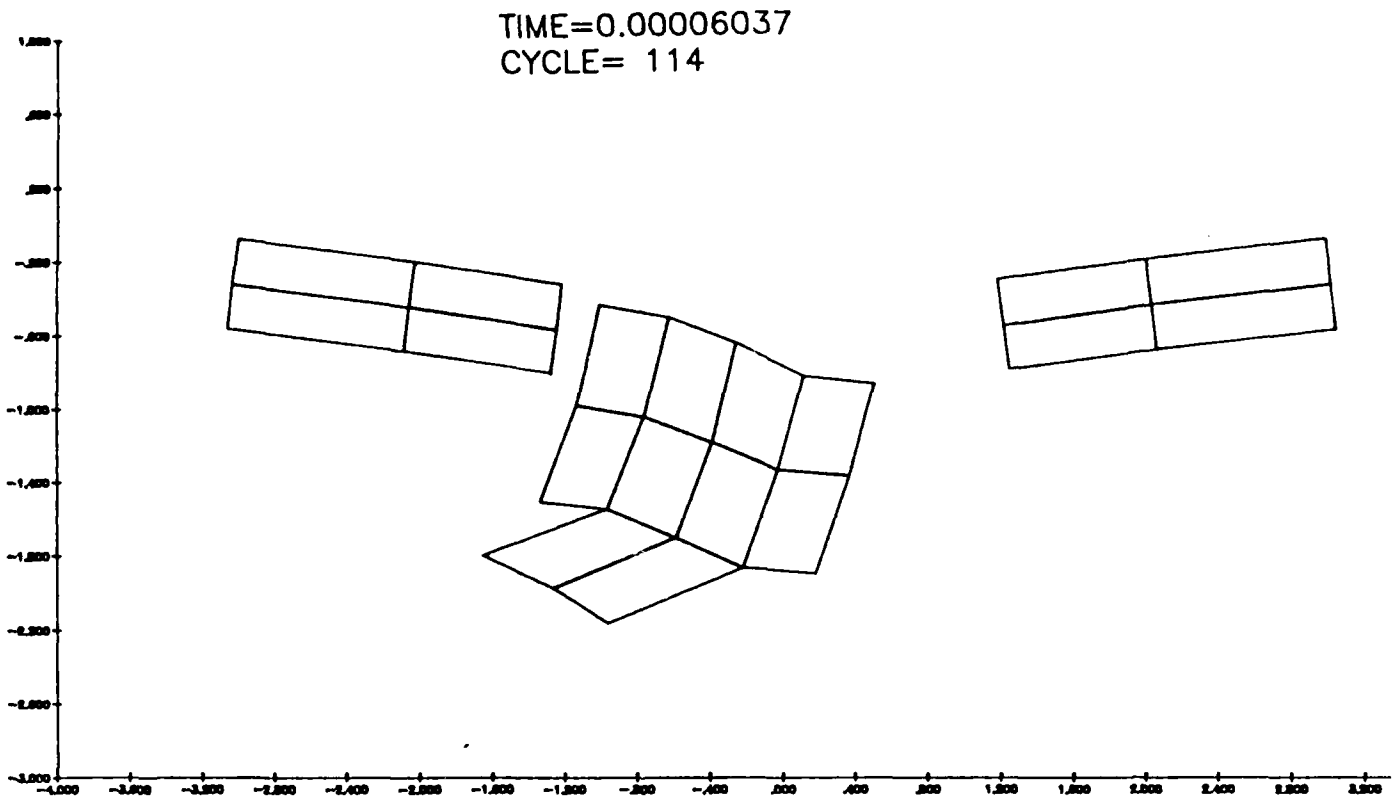

Fig. 9c Evolution of mesh for example 1

DISTRIBUTION LIST

No. of Copies	Organization
12	Administrator Defense Technical Info Center ATTN: DTIC-DDA Cameron Station Alexandria, VA 22314
1	Director Defense Advanced Research Projects Agency ATTN: Tech Info 1400 Wilson Boulevard Arlington, VA 22209
1	Director Defense Nuclear Agency Arlington, VA 22209
1	Deputy Assistant Secretary of the Army (R&D) Department of the Army Washington, DC 20301
2	Commander US Army BMD Advanced Technology Center ATTN: BMDATC-M, Mr. P. Boyd Mr. S. Brockway PO Box 1500 Huntsville, AL 35807
1	HQDA (DAMA-ARP) Wash DC 20310
1	HQDA (DAMA-MS) Wash DC 20310
2	Commander US Army Engineer Waterways Experiment Station ATTN: Dr. P. Hadala Dr. B. Rohani PO Box 631 Vicksburg, MS 39180
1	Commander US Army Materiel Command ATTN: AMCDRA-ST 5001 Eisenhower Avenue Alexandria, VA 22333
10	Commander Armament R&D Center US Army AMCCOM ATTN: SMCAR-TSS SMCAR-TDC SMCAR-TD, Dr. Weigle SMCAR-LC, Dr. Frasier SMCAR-SC, Dr. Gyorog SMCAR-LCF, G. Demitrack SMCAR-LCA, G. Randers-Pehrson SMCAR-SCS-M, R. Kwatnoski SMCAR-LCU, E. Barrieres SMCAR-SCM, Dr. Bloore Dover, NJ 07801
2	Director US Army AMCCOM, ARDC Benet Weapons Laboratory ATTN: SMCAR-LCB-TL Dr. J. E. Flaherty Watervliet, NY 12189
1	Commander US Army Armament, Munitions and Chemical Command ATTN: SMCAR-ESP-L, Tech Lib Rock Island, IL 61299
1	Commander US Army Aviation Research and Development Command ATTN: AMSAV-E 4300 Goodfellow Blvd. St. Louis, MO 63120
1	Director US Army Air Mobility Research and Development Laboratory Ames Research Center Moffett Field, CA 94035
1	Commander US Army Communications Electronics Command ATTN: AMSEL-ED Fort Monmouth, NJ 07703
1	AFWL/SUL Kirtland AFB, NM 87117

REFERENCES

1. T. Belytschko, W.K. Liu, J.M. Kennedy and S.J. Ong, "Hourglass Control in Linear and Nonlinear Problems," to appear Computer Methods in Applied Mechanics and Engineering.

2. D.P. Flanagan and T. Belytschko, "A Uniform Strain Hexahedron and Quadrilateral with Orthogonal Hourglass Control," International Journal for Numerical Methods in Engineering, 17, 679-706, 1981.

3. G.L. Goudreau and J.O. Hallquist, "Recent Development in Large Scale Finite Elements Lagrangian Hydrocode Technology," Report UCRL-86460. Lawrence Livermore Laboratory, October 1981, Nos. 1-3, September 1982, Vol. 33.

4. D.P. Flanagan and T. Belytschko, "Eigenvalues and Stable Time Steps for the Uniform Strain Hexahedron and Quadrilateral," Journal of Applied Mechanics, Trans. ASME, Vol. 51, pp 35-40, March 1984.

5. T. Belytschko, "An Overview of Semidiscretization and Time Integration Procedure," Chapter 1 in Computational Methods for Transient Analysis, ed. by T. Belytschko and T.J.R. Hughes, North-Holland, 1983.

6. G.R. Johnson, "EPIC-3, A Computer Program for Elastic-Plastic Impact Calculations in 3 Dimensions," BRL 343, AD-058786, Honeywell Inc., Defense Systems Div., Hopkins, Minn., July 1977.

7. G.R. Johnson, D.D. Colby and D.J. Vavrick, "Further Development of the EPIC-3 Computer Program for Three-Dimensional Analysis of Intense Impulsive Loading," Report AFATL-TR-78-81, 1978.

Table 8

MAIN ROUTINE INPUT DATA

DESCRIPTION CARD (12A6)

Description of Problem	

IDENTIFICATION CARD (3I5,5X,F10.0,E15.8,5X,F10.0)

CASE	CYCLE	IPRES		CPMAX	EMAX		HGMAX	

INTEGRATION TIME INCREMENT CARD AND CELL STRUCTURE (7F10.0)

DTMAX	DTMIN	SSF	TMAX	XDIS	YDIS	ZDIS	

CELL PARAMETER CARD (6E10.3)

SXMAX	SXMIN	SYMAX	SYMIN	SZMAX	SZMIN	

If NX1 = 1, NX2 = NLX, NY2 = NLY and NZ2 - NLZ-1, all elements in the target are master elements.

Main

Identification Card (3I5, 5X, F10.0, E15.8, F10.3) - Add one additional parameter SFAIL in column 51-60.

SFAIL: hourglass failure criterion; (10.0 ~12.0 is recommended)

Integration Time Increment Card (8F10.0) -

column	variable name	description
1 - 10	DTMAX	maximum time step
11 - 20	DTMIN	minimum time step
21 - 30	SSF	time step safety factor, < 1.0
31 - 40	TMAX	time problem is allowed to run
41 - 50	HRCON	hourglass control factor, 0.05 to 0.2 is recommended.
51 - 60	XDIS	size in x-direction for a cell
61 - 70	YDIS	size in y-direction for a cell
71 - 80	ZDIS	size in z-direction for a cell

Cell Parameter Card (6E10.3) - See Section 2.2

This card should follow right after the Integration Time Increment Card.

column	variable name	description
1 - 10	SXMAX	x_{max}
11 - 20	SXMIN	x_{min}
21 - 30	SYMAX	y_{max}
31 - 40	SYMIN	y_{min}
41 - 50	SZMAX	z_{max}
51 - 60	SZMIN	z_{min}

Only the metallic material (material code = 1) can be used. The input format for the Main Program is summarized in Table 8.

Postprocessor

Only the plane of symmetry can be plotted when the hexahedra and erosion features are used.

Section 4

INPUT FORMAT

The input format is almost identical to that of the original EPIC-3 code [6,7]. The major differences are that the cell description has been added to the integration time increment card and a subsequent card, and there are some restrictions on the features which can be used with the hexahedron and erosion.

The following restrictions apply to the hexahedron and erosion interface:

1. the erosion interface can not be used with tetrahedral elements;
2. the anisotropic material cannot be used with the hexahedra.

Preprocessor

The master elements must be identified through the element description cards. This is accomplished by specifying MIDEN in columns 61-65 for the composite-element-description cards or columns 31-35 for any other element description cards. MIDEN is specified as follows:

MIDEN = 0 (or blank) if the element is not a master element
MIDEN = 1 if the element is a master but not on the bottom layer
MIDEN = 2 if the element is a master on the bottom layer of the target

For a plate target, MIDEN can be generated automatically if the master elements are to occupy a regular domain in the target. Recall that the flat-plate target consists of NLX layers of elements in the x-direction, NLY layers in the y-direction, and NLZ layers in the z-direction. We assign numbers to the layers beginning with lowest value of the coordinate and in the direction in which the coordinate increases. The master elements identification (MIDEN) can then be generated automatically whenever all elements between layers NX1 and NX2 in the x-direction, between layers 1 and NY2 in the y-direction, and layers 1 and NZ2 in the z-direction are master elements. In that case, columns 31-35 of the flat-plate element description card are as follows:

Flat Plate Description Card

Columns	Variable Name	Description
31-35	MIDEN	leave blank when automatic generation of MIDEN is to be used.
36-40	NX1	lowest layer number for master elements in x-direction
41-45	NX2	largest layer number for master elements in x-direction
46-50	NY2	largest layer number for master elements in y-direction
51-55	NZ2	largest layer number for master elements in z-direction

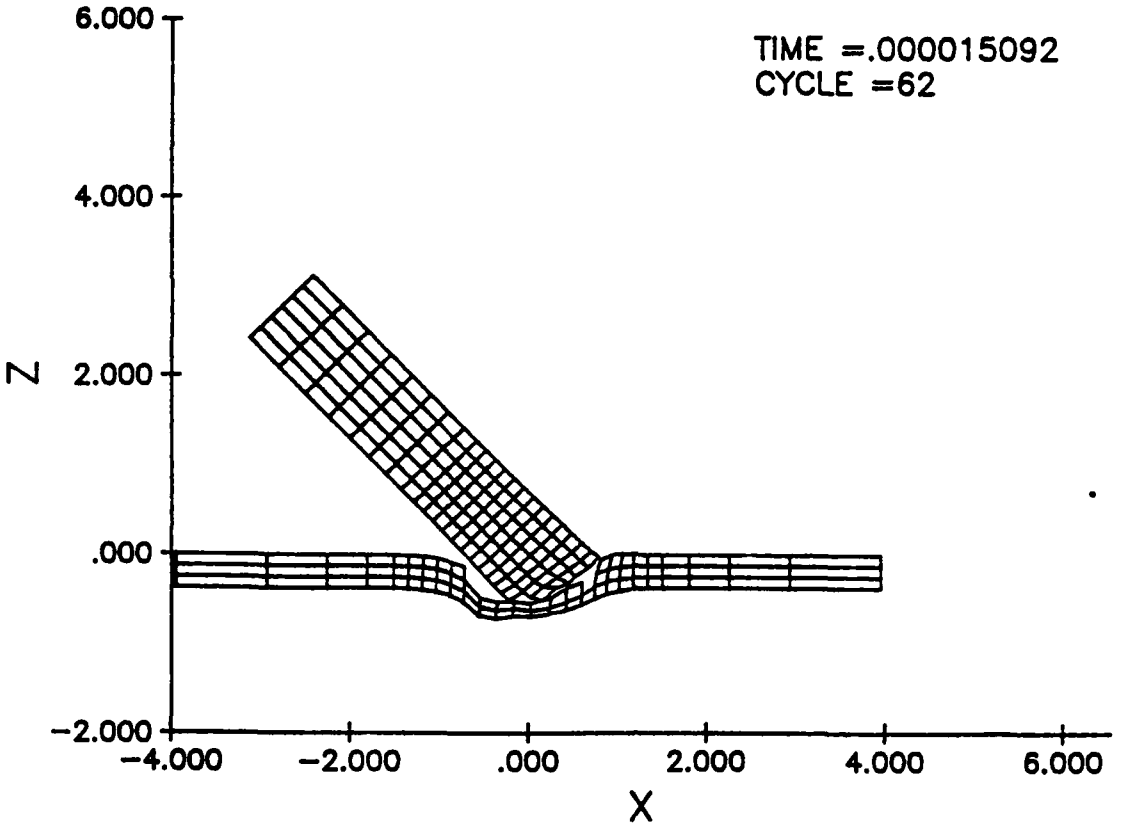

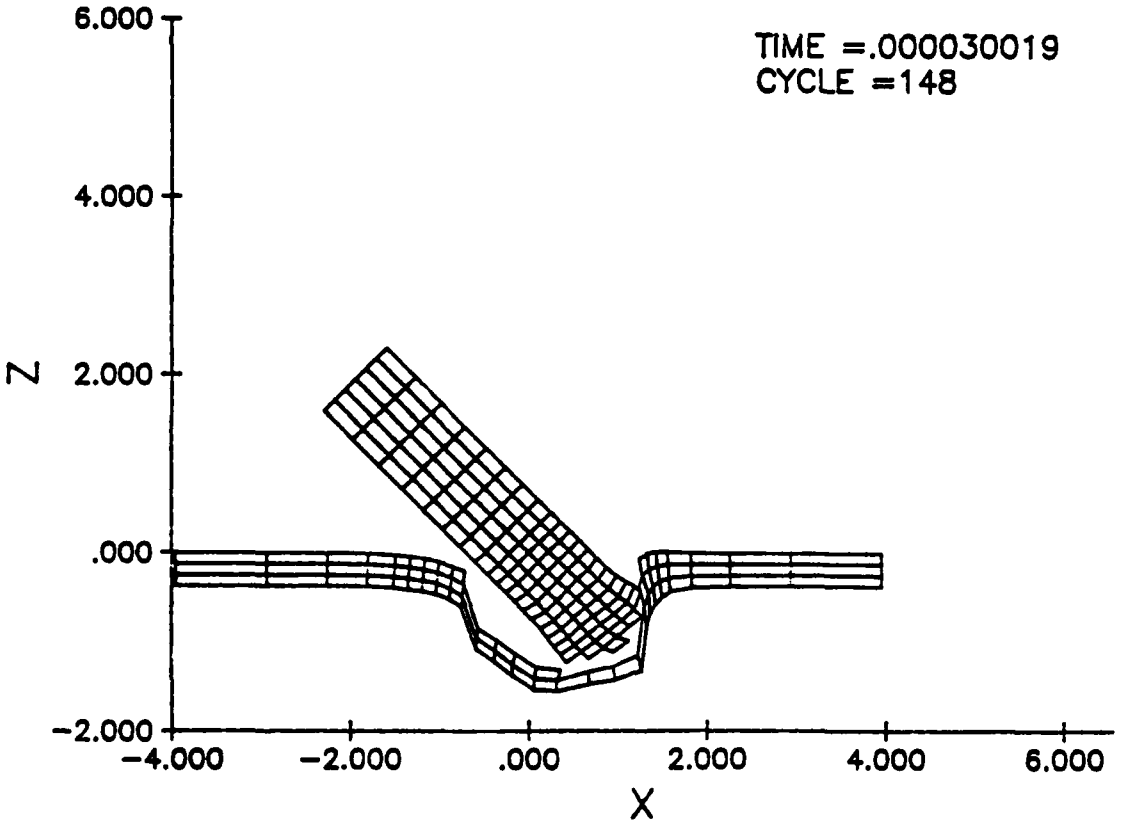

Fig. 11b Evolution of mesh on plane symmetry for example 3.

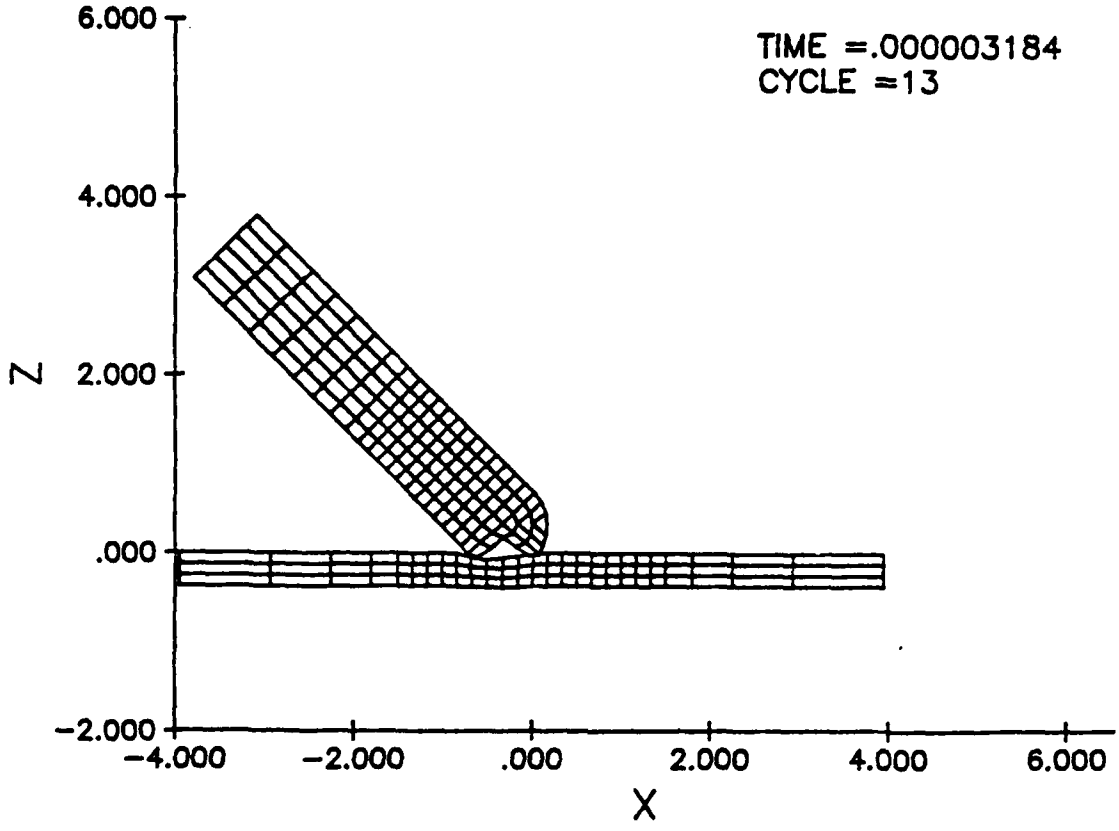

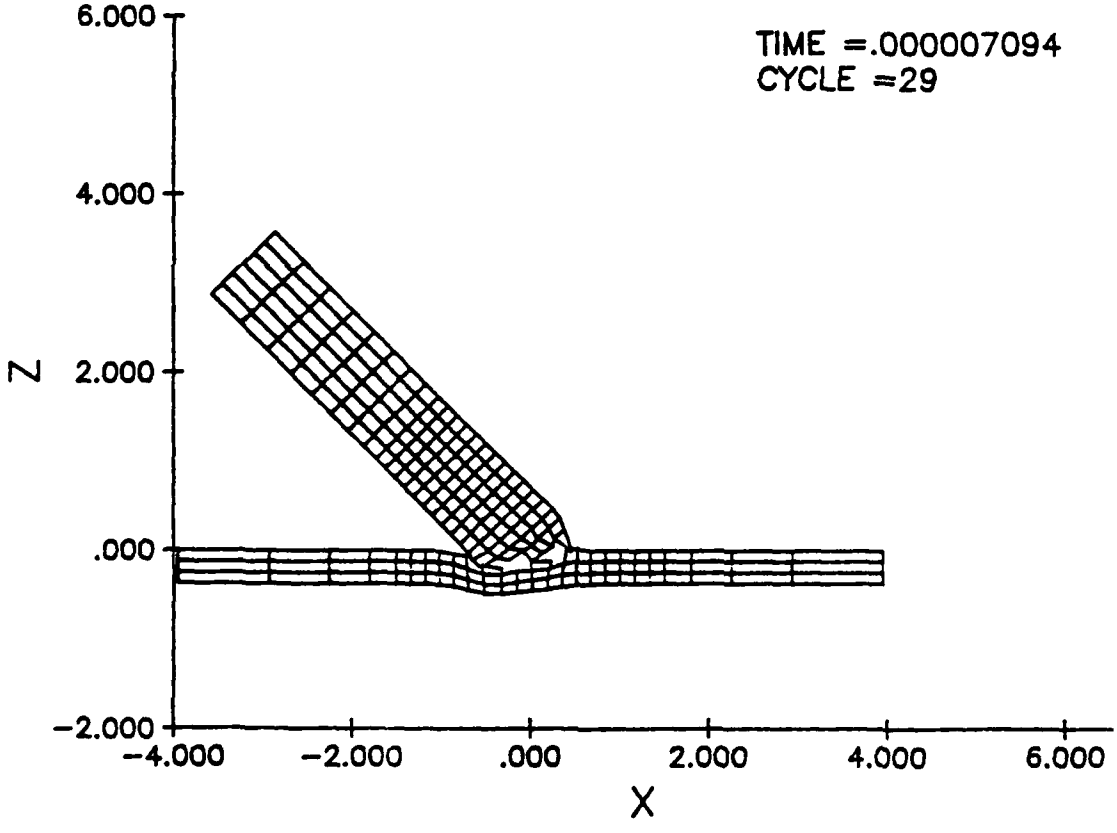

Fig. 11a Evolution of mesh on plane of symmetry for example 3.

Table 7 Continued

```
>5 DEGREES PENETRATION (SAMPLE IN EPIC3 MANUAL)
   1     1     1     1                              1     3          21
   1     1
  .000831     360000. 20739000. 32907000. 64234000.          2.          .2  4.
6380000.      20300.    65300.        .3 9999999.           0.          1.  0.
     999.        999.        2.        0.
   3     1
  .000734     410000. 24200000. 59578000. 74081000.        1.67          .2  4.
9300000.      160000.   203000.        .3 9999999.           0.          1.  0.
     999.          .7       999.        0.

       1.          1.          1.        0.         .21       -45.
   2
   3     0     8     0         4.9       2.5          .9
       .5          0.          .5        0.
   2
   3     0    13     0         2.3        .5         1.0
       .5          0.          .5        0.
   3
   3     0     2     0          .5        0.          .5         0.

       1.          1.          1.
   4     2
  27    14     4     5     0     1         1.5         .31        1.0         0.0  1.1
    -3.95          0.          0.        3.95        3.95       -.375

   2
   3     1    20     1     0     1
   3
   3     1          589     0     1

   4     2
  26    13     3   673           3     1     3    22     7     2

   1     3     2   677   281   672   392     0     0                 0.    200000.
  10    10     1    27     1


  55660.          0.   -55660.          0.          0.          0. .00000001
```

TABLE 7

Parameters and input for Example 3

Projectile

shape	:	rod with a round nose
dimensions	:	4.9 in long, 0.5 in radius
density	:	0.000831 lb-sec^2/in^4
bulk modulus	:	20,739,000 psi
shear modulus	:	6,380,000 psi
yield stress	:	20,300 psi
ultimate stress	:	65,300 psi
initial velocity	:	x-component 55660.0 in/sec z-component -55660.0 in/sec

Target

shape	:	plate
dimensions	:	7.9 in x 3.95 in x 0.375 in (half plate)
density	:	0.000734 lb-sec^2/in^4
bulk modulus	:	24,200,000 psi
shear modulus	:	9,300,000 psi
yield stress	:	160,000 psi
ultimate stress	:	203,000 psi
initial velocity	:	0

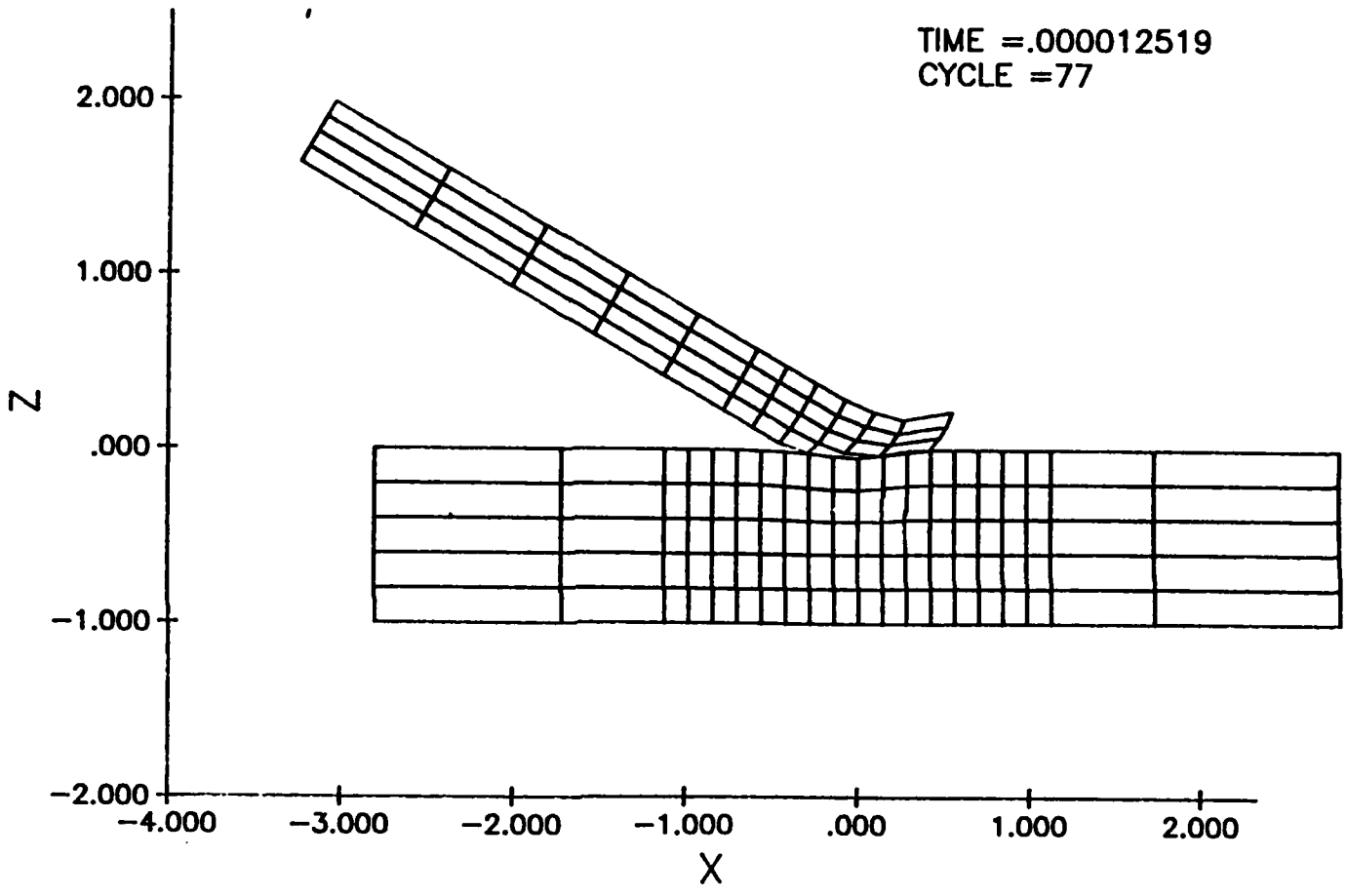

Fig. 10c Evolution of mesh for example 2

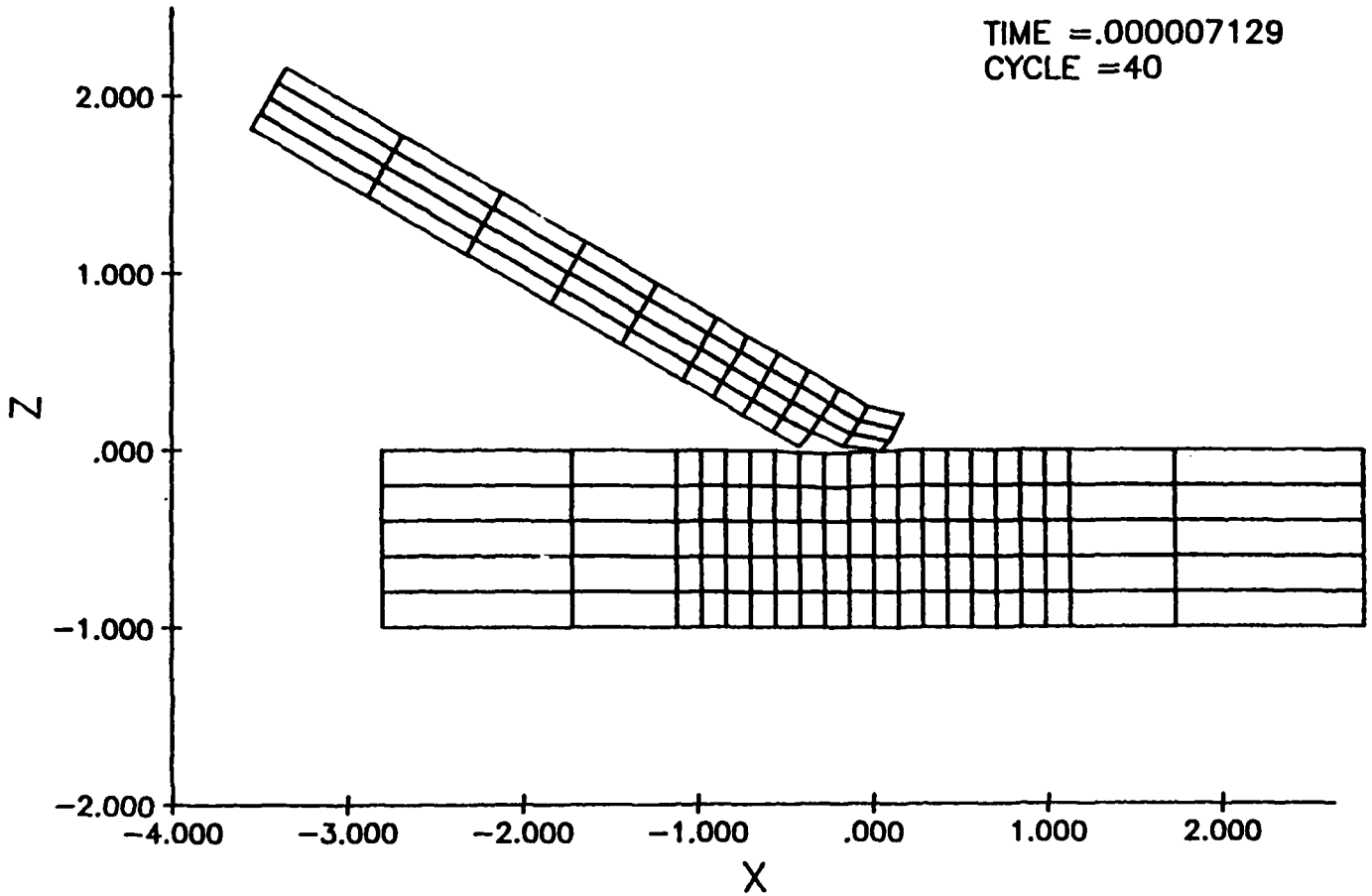

Fig. 10b Evolution of mesh for example 2

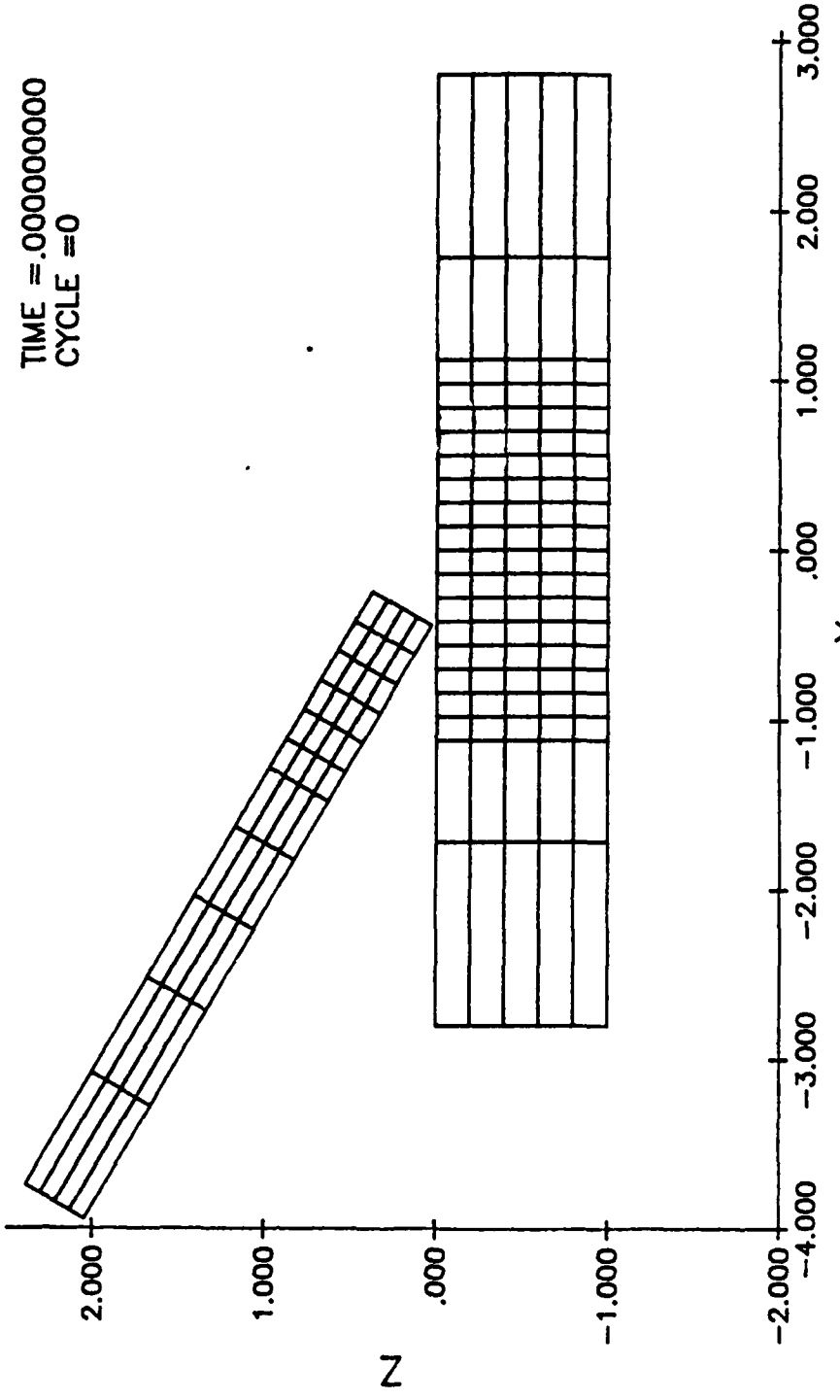

Fig. 10a Evolution of mesh for example 2

Table 6 Continued

```
60 DEGREE PENETRATION
701     1     1
  1     1   PROJECTILE MATERAL
 0.00073   410000.0 23810000.
11630000.    250000.    310000.          0.3   9999999.          0.0          1.0
     999.         0.4         1.6         0.0
  2     1   TARGET MATERAL
 0.00073   410000.0 27790000.
11360000.    160000.    185000.          0.3   9999999.                       1.0
     999.         0.3         0.6         0.0

     1.0          1.0          1.0         0.0       0.400       -60.0
  2
  2     0     6     0          4.04         1.2         0.35
   0.201          0.0        0.201         0.0
  2
  2     0     6     0          1.0          0.0          1.0
   0.201          0.0        0.201         0.0

     1.0          1.0          1.0
  4     2
 21     6     6     3     0     1           1.8          0.3          1.0          0.0  1.0
    -2.8          0.0          0.0         2.8          0.7         -1.0

  2
  2     1    11     1     0     1     0

  4     2
 20     5     5   181           2     1     5    17     3     4

  1     3     1   181    76   180   105     0     0                  0.0          1.0  1.0
 14     4     1   126

    56155.          0.0     -32421.          0.0          0.0          0.0.000000006
```

TABLE 6

Parameters and input for Example 2

Projectile		
shape	:	rod
dimensions	:	4.04 in long, 0.201 in radius
density	:	0.00073 lb-sec^2/in^4
bulk modulus	:	23,810,000 psi
shear modulus	:	11,630,000 psi
yield stress	:	250,000 psi
ultimate stress	:	310,000 psi
initial velocity	:	x-component 56155.0 in/sec z-component -32421.0 in/sec
Target		
shape	:	plate
dimensions	:	5.6 in x 0.7 in x 1 in (half plate)
density	:	0.00073 lb-sec^2/in^4
bulk modulus	:	27,780,000 psi
shear modulus	:	11,360,000 psi
yield stress	:	160,000 psi
ultimate stress	:	185,000 psi
initial velocity	:	0

DISTRIBUTION LIST

No. of Copies	Organization
1	Commander US Army Electronics Research and Development Command Technical Support Activity ATTN: DELSD-L Fort Monmouth, NJ 07703-5301
1	Commander US Army Missile Command ATTN: AMSMI-R Redstone Arsenal, AL 35898
2	Commander US Tank Automotive Command ATTN: AMSTA-TSL V. H. Paganp Warren, MI 48090
1	Program Manager M1 Abrams Tank System ATTN: AMCPM-GCM-SA, T. Dean Warren, MI 48090
1	Commander US Army Missile Command ATT. AMSMI-YDL Redstone Arsenal, AL 35898
1	Commander US Army Missile Command ATTN: AMSMI-RBL Redstone Arsenal, AL 35898
6	Director US Army Materials and Mechanics Research Center ATTN: AMXMR-T, Mr. J. Bluhm Mr. J. Mescall Dr. M. Lenoe R. Shea F. Quigley AMXMR-ATL Watertown, MA 02172
2	Commander US Army Research Office ATTN: Dr. E. Saibel Dr. G. Mayer PO Box 12211 Research Triangle Park NC 27709-2211
1	HQDA DAMA-ART-M Washington, DC 20310
1	Director US Army, TRADOC Systems Analysis Activity ATTN: ATTA-SL (Tech Lib) White Sands Missile Range NM 88002
1	Office of Naval Research Department of the Navy ATTN: Code ONR 439, N. Perrone 800 North Quincy Street Arlington, VA 22217
3	Commander Naval Air Systems Command ATTN: AIR-604 Washington, DC 20360
3	Commander Naval Ordnance Systems Command Washington, DC 20360
2	Commander Naval Air Development Center, Johnsville Warminster, PA 18974
1	Commander Pacific Naval Missile Test Center Point Mugu, CA 93042
1	Naval Ship Engineering Center ATTN: Tech Lib Washington, DC 20362
1	Commander & Director David W. Taylor Naval Ship Research & Development Center ATTN: Code 1740.4, R. A. Gramm Bethesda, MD 20084
1	Commandant US Army Infantry School ATTN: ATSH-CD-CSO-OR Fort Benning, GA 31905

DISTRIBUTION LIST

No. of Copies	Organization
3	Commander Naval Surface Weapons Center ATTN: Dr. W. G. Soper Mr. N. Rupert Code G35, D. C. Peterson Dahlgren, VA 22448
10	Commander Naval Surface Weapons Center ATTN: Dr. S. Fishman (2 cys) Code R-13, F. J. Zerilli K. Kim E. T. Toton M. J. Frankel Code U-11, J. R. Renzi R. S. Gross Code K-22, F. Stecher J. Etheridge Silver Spring, MD 20910
3	Commander Naval Weapons Center ATTN: Code 31804, Mr. M. Smith Code 326, Mr. P. Cordle Code 3261, Mr. T. Zulkoski China Lake, CA 93555
6	Commander Naval Weapons Center ATTN: Code 3181, John Morrow Code 3261, Mr. C. Johnson Code 3171, Mr. B. Galloway Code 3831, Mr. M. Backman Mr. R.E. VanDevender, Dr. O. E. R. Heimdahl China Lake, CA 93555
2	Director Naval Research Laboratory ATTN: Anacostia Station Dr. C Sanday Dr. H. Pusey Washington, DC 20375
2	Superintendent Naval Postgraduate School ATTN: Dir of Lib Dr. R. Ball Monterey, CA 93940
3	Long Beach Naval Shipyard ATTN: R. Kessler T. Eto R. Fernandez Long Beach, CA 90822
1	HQ USAF/SAMI Washington, DC 20330
1	AFIS/INOT Washington, DC 20330
1	ADTC/DLJW (LT K. Ols) Eglin AFB, FL 32542
1	ADTC/DLYV (Mr. J. Collins) Eglin AFB, FL 32542
1	AFATL/DLYV Eglin AFB, FL 32542
1	AFATL/DLODL Eglin AFB, FL 32542
1	AFATL/CC Eglin AFB, FL 32542
1	AFATL/DLODR Eglin AFB, FL 32542
1	HQ PACAF/DOOQ Hickam AFB, HI 96853
1	HQ PACAF/OA Hickam AFB, HI 96853
1	OOALC/MMWMC Hill AFB, UT 84056
1	HQ TAC/DRA Langley AFB, VA 23365

DISTRIBUTION LIST

No. of Copies	Organization
1	AUL-LSE 71-249 Maxwell AFB, AL 36112
1	AFWAL/MLLN (Mr. T. Nicholas) Wright-Patterson AFB, OH 45433
1	ASD/ENESS (S. Johns) Wright-Patterson AFB, OH 45433
1	ASD/ENFEA Wright-Patterson AFB, OH 45433
1	ASD/XRP Wright-Patterson AFB, OH 45433
1	HQUSAFE/DOQ APO New York 09012
1	COMIPAC/I-32 Box 38 Camp H. I. Smith, HI 96861
10	Battelle Pacific Northwest Laboratories PO Box 999 ATTN: G. D. Marr Richland, WA 99352
4	Lawrence Livermore Laboratory PO Box 808 ATTN: Dr. R. Werne Dr. J. O. Hallquist Dr. M. L. Wilkins Dr. G. Goudreau Livermore, CA 94550
5	Director Los Alamos Scientific Laboratory PO Box 1663 ATTN: Dr. R. Karpp Dr. J. Dienes Dr. E. Fugelso Dr. D. E. Upham Dr. R. Keyser Los Alamos, NM 87544
6	Sandia National Laboratory ATTN: Dr. R. Woodfin Dr. M. Sears Dr. W. Herrmann Dr. L. Bertholf Dr. A. Chabai Dr. C. B. Selleck Albuquerque, NM 87115
1	Commander US Army Development and Employment Agency ATTN: MODE-TED-DAB Fort Lewis, WA 98433
1	Director Jet Propulsion Laboratory 4800 Oak Grove Drive ATTN: Dr. Ralph Chen Pasadena, CA 91109
1	Director National Aeronautics and Space Administration Langley Research Center Langley Station Hampton, VA 23365
1	Director US Geological Survey 2255 N. Gemini Drive ATTN: Dr. D. Roddy Flagstaff, AZ 86001
1	AAI Corporation PO Box 6767 ATTN: R. L. Kachinski Baltimore, MD 21204
1	Aerojet Ordnance Company 9236 East Hall Road Downey, CA 90241
1	Aeronautical Research Associates of Princeton, Inc. 50 Washington Road P.O. Box 2229 Princeton, NJ 08540

DISTRIBUTION LIST

No. of Copies	Organization
1	Aerospace Corporation 2350 E. El Segundo Blvd. ATTN: Mr. L. Rubin El Segundo, CA 90245
1	AVCO Systems Division 201 Lowell Street ATTN: Dr. Reinecke Wilmington, MA 01887
3	Battelle Columbus Laboratories 505 King Avenue ATTN: Dr. G. T. Hahn Dr. L. E. Hulbert Dr. S. Sampath Columbus, OH 43201
4	Boeing Company Aerospace Division ATTN: Mr. R. G. Blaisdell (M.S. 40-25) Dr. N. A. Armstrong, C. J. Artura (M.S. 8C-23) Dr. B. J. Henderson (M.S. 43-12) Seattle, WA 98124
2	Brunswick Corporation 4300 Industrial Avenue ATTN: P. S. Chang R. Grover Lincoln, NE 68504
1	Computer Code Consultants, Inc. 1680 Camino Redondo ATTN: Dr. Wally Johnson Los Alamos, NM 87544
1	Dresser Center PO Box 1407 ATTN: Dr. M. S. Chawla Houston, TX 77001
1	Effects Technology, Inc. 5383 Hollister Avenue Santa Barbara, CA 93111
1	Electric Power Research Institute PO Box 10412 ATTN: Dr. George Sliter Palo Alto, CA 94303
1	FMC Corporation Ordnance Engineering Division San Jose, CA 95114
1	Ford Aerospace and Communications Corporation Ford Road, PO Box A ATTN: L. K. Goodwin Newport Beach, CA 92663
1	General Dynamics PO Box 2507 ATTN: J. H. Cuadros Pomona, CA 91766
1	General Electric Company Lakeside Avenue ATTN: D. Graham, RM 1311 Burlington, VT 05401
1	President General Research Corporation ATTN: Lib McLean, VA 22101
1	Goodyear Aerospace Corporation 1210 Massillon Road Akron, OH 44315
1	H. P. White Laboratory 3114 Scarboro Road Street, MD 21154
5	Honeywell, Inc. Government and Aerospace Products Division ATTN: Mr. J. Blackburn Dr. G. Johnson Mr. R. Simpson Mr. K. H. Doeringsfeld Dr. D. Vavrick 600 Second Street, NE Hopkins, MN 55343

DISTRIBUTION LIST

No. of Copies	Organization
1	Hughes Aircraft Corporation ATTN: MS M-5, Bldg 808 Tucson, AZ 85706
2	Kaman Sciences Corporation 1500 Garden of the Gods Road ATTN: Dr. P. Snow Dr. D. Williams Colorado Springs, CO 80907
1	Lockheed Palo Alto Research Laboratory 3251 Hanover Street ATTN: Org 5230, Bldg 201 Mr. R. Robertson Palo Alto, CA 94304
1	Lockheed Missiles and Space Company PO Box 504 ATTN: R. L. Williams Dept. 81-11, Bldg 154 Sunnyvale, CA 94086
1	Materials Research Laboratory, Inc. 1 Science Road Glenwood, IL 60427
2	McDonnell-Douglas Astronautics Company 5301 Bolsa Avenue ATTN: Dr. L. B. Greszczuk Dr. J. Wall Huntington Beach, CA 92647
1	New Mexico Institute of Mining and Technology ATTN: TERA Group Socorro, NM 87801
1	Northrup Corporation 3901 W. Broadway ATTN: R. L. Ramkumar Hawthorne, CA 90250
1	Nuclear Assurance Corporation 24 Executive Park West ATTN: T. C. Thompson Atlanta, GA 30245
2	Orlando Technology, Inc. PO Box 855 ATTN: Mr. J. Osborn Mr. D. Matuska Shalimar, FL 32579
1	Rockwell International Autometrics Missile Systems Division ATTN: A. R. Claser 4300 E. Fifth Avenue Columbus, OH 43216
3	Schumberger Well Services Perforating Center ATTN: J. E. Brooks J. Brookman Dr. C. Aseltine PO Box A Rosharon, TX 77583
1	Science Applications, Inc. 101 Continental Boulevard Suite 310 El Segundo, CA 90245
1	Systems, Science and Software PO Box 1620 ATTN: Dr. R. Sedgwick La Jolla, CA 92038
2	Ted Belytschko Inc. ATTN: T. Belytschko J. I. Lin 18 Longmeadow Road Winnetka, IL 60093

DISTRIBUTION LIST

No. of Copies	Organizations
2	TRW One Space Park, 134/9048 ATTN: D. Ausherman M. Bronstein Redondo Beach, CA 90278
1	United Technologies Research Center 438 Weir Street ATTN: P. R. Fitzpatrick Glastonbury, CT 06033
1	US Steel Corporation Research Center 125 Jamison Center Monroeville, PA 15146
1	VPI & SU 106C Norris Hall ATTN: Dr. M. P. Kamat Blacksburg, VA 24061
2	Vought Corporation PO Box 225907 ATTN: Dr. G. Hough Dr. Paul M. Kenner Dallas, TX 75265
1	Westinghouse, Inc. PO Box 79 ATTN: J. Y. Fan W. Mifflin, PA 15122
1	Drexel University Department of Mechancial Engr. ATTN: Dr. P. C. Chou 32d and Chestnut Streets Philadelphia, PA 19104
5	Southwest Research Institute Dept. of Mechanical Sciences ATTN: Dr. U. Lindholm Dr. W. Baker Dr. R. White Dr. M. F. Kanninen Dr. C. Anderson 8500 Culebra Road San Antonio, TX 78228
4	SRI International 333 Ravenswood Avenue ATTN: Dr. L. Seaman Dr. L. Curran Dr. D. Shockey Dr. A. L. Florence Menlo Park, CA 94025
2	University of Arizona Civil Engineering Department ATTN: Dr. D. A. DaDeppo Dr. R. Richard Tucson, AZ 85721
1	University of Arizona School of Engineering ATTN: Dean R. Gallagher Tucson, AZ 85721
1	University of Denver Denver Research Institute ATTN: Mr. R. F. Recht 2390 S. University Blvd Denver, CO 80210
1	University of California Department of Physics ATTN: Dr. Harold Lewis Santa Barbara, CA 93106
2	University of California College of Engineering ATTN: Prof. W. Goldsmith Dr. A. G. Evans Berkeley, CA 94720
2	University of Delaware Department of Mechanical Engineering ATTN: Prof. J. Vinson Prof. B. Pipes Newark, DE 19711

DISTRIBUTION LIST

No. of Copies	Organization
2	University of Florida Department of Engineering Sciences ATTN: Dr. R. L. Sierakowski Dr. L. E. Malvern Gainesville, FL 32601
1	University of Oklahoma School of Aerospace, Mechanical and Nuclear Engineering ATTN: Dr. C. W. Bert Norman, OK 73069

Aberdeen Proving Ground

Dir, USAMSAA
ATTN: AMXSY-D
AMXSY-MP, H. Cohen
Cdr, USATECOM
ATTN: AMSTE-TO-F
Cdr, USACSTA
ATTN: Mr. S. Keithley

Cdr, CRDC, AMCCOM
ATTN: SMCCR-RSP-A
SMCCR-MU
SMCCR-SPS-IL

USER EVALUATION SHEET/CHANGE OF ADDRESS

This Laboratory undertakes a continuing effort to improve the quality of the reports it publishes. Your comments/answers to the items/questions below will aid us in our efforts.

1. BRL Report Number _____ Date of Report _____

2. Date Report Received _____

3. Does this report satisfy a need? (Comment on purpose, related project, or other area of interest for which the report will be used.) _____

_____

_____

4. How specifically, is the report being used? (Information source, design data, procedure, source of ideas, etc.) _____

_____

_____

5. Has the information in this report led to any quantitative savings as far as man-hours or dollars saved, operating costs avoided or efficiencies achieved, etc? If so, please elaborate. _____

_____

_____

6. General Comments. What do you think should be changed to improve future reports? (Indicate changes to organization, technical content, format, etc.)

_____

_____

_____

CURRENT ADDRESS

_____
Name

_____
Organization

_____
Address

_____
City, State, Zip

7. If indicating a Change of Address or Address Correction, please provide the New or Correct Address in Block 6 above and the Old or Incorrect address below.

OLD ADDRESS

_____
Name

_____
Organization

_____
Address

_____
City, State, Zip

(Remove this sheet along the perforation, fold as indicated, staple or tape closed, and mail.)

FOLD HERE

:or
ny Ballistic Research Laboratory
AMXBR-OD-ST
:een Proving Ground, MD 21005-5066

NO POSTAGE
NECESSARY
IF MAILED
IN THE
UNITED STATES

FFICIAL BUSINESS
TY FOR PRIVATE USE, $300

BUSINESS REPLY MAIL
FIRST CLASS PERMIT NO 12062 WASHINGTON, DC
POSTAGE WILL BE PAID BY DEPARTMENT OF THE ARMY

Director
US Army Ballistic Research Laboratory
ATTN: AMXBR-OD-ST
Aberdeen Proving Ground, MD 21005-9989

FOLD HERE